Development of a Physically Based Sediment Transport Model for Green Bay, Lake Michigan

Bahram Khazaei[1,2], Hector R. Bravo[1], Eric J. Anderson[3], and Jeffrey V. Klump[4]

[1] Department of Civil and Environmental Engineering, University of Wisconsin-Milwaukee

[2] Research Applications Laboratory, National Center for Atmospheric Research

[3] Great Lakes Environmental Research Laboratory, National Oceanic and Atmospheric Administration

[4] School of Freshwater Sciences, University of Wisconsin-Milwaukee

Corresponding author: Hector R. Bravo (hrbravo@uwm.edu)

Key Points:

- Understanding the simultaneous effects of tributary flows and lake intrusions is crucial to comprehend the dynamics of freshwater estuaries
- The circulation, thermal regime, wave action, and sediment transport in the estuary depend on meteorological forcing, tributary flows, and lake intrusions
- The stage is set to apply this approach to study biogeochemical processes in lakes and estuaries

Abstract

Green Bay is the largest freshwater estuarine system on earth, drains one-third of the Lake Michigan basin and delivers one-third of the lake's phosphorus load. Southern Green Bay is a designated area of concern (AOC) due to ecosystem degradation that includes eutrophication, harmful algal blooms (HABs), hypoxia, lost or altered habitat, and reduced water quality. While marine estuaries are subject to tidal influence and saltwater intrusion, this freshwater estuary is subject to lake intrusion of freshwater with different quality parameters. Understanding the simultaneous effects of tributary flows and lake intrusions is crucial to comprehend the dynamics of freshwater estuaries. A single hydrodynamic, wind-wave, and sediment transport model was developed for the lake and its estuary. This approach provides fine resolution in the estuary and simulates directly the combined effects of tributary flows and lake intrusions. The approach overcomes open-boundary limitations of nested models, and of whole-lake models that lack sufficient resolution or wind-wave and sediment transport simulation. The model confirms findings of previous studies and demonstrates how the circulation, thermal regime, wave action, and sediment transport in the estuary depend on meteorological forcing, tributary flows, and lake intrusions. The stage is set to apply this approach to study biogeochemical processes in lakes and estuaries.

Keywords: Green Bay, freshwater estuaries, sediment transport, physically-based models.

Plain Language Summary

Green Bay is a unique ecosystem located in the largest freshwater system on earth, the Laurentian Great Lakes. Almost one-third of tributary waters to Lake Michigan flow through Green Bay. Human activities in the watershed produce excessive amounts of contaminated and/or nutrient-rich sediments that are discharged to the bay. Sediments are not efficiently transported to Lake Michigan due to physical conditions in Green Bay, leading to ecosystem degradation, environmental and public health risks. We studied the movement, transport, and fate of sediments in Lake Michigan, with a special attention to Green Bay, by developing a physically-based, 3D sediment transport model. This model development effort helps to predict circulation of contaminants and nutrients that are attached to the sediments, their settlement and burial, and the detachment from the bottom during storm events. The knowledge gained in this study will enhance our understanding of water quality conditions and nutrient recycling in freshwater estuaries, and will improve future restoration efforts and management plans.

1 Introduction

Green Bay is the largest freshwater estuarine system on earth, drains one-third of Lake Michigan basin and delivers one-third of the lake's total phosphorus load (Klump et al., 2018). The International Joint Commission designated southern Green Bay as an area of concern (AOC) in the 1980s due to several instances of ecosystem degradation including (but not limited to) eutrophication, harmful algal blooms (HABs), hypoxia, lost or altered habitat, and reduced water quality.

Green Bay has stimulated a significant amount of widely relevant research on the fate and behavior of toxics, biogeochemistry, habitat, biodiversity, and ecological processes. In particular, previous research relevant to hydrodynamics and sediment transport in Green Bay includes studies carried out on Green Bay, studies done on Lake Michigan and the Laurentian Great Lakes watershed, and studies done on marine estuaries. We will first concisely list those previous studies, then briefly explain how the present study differs in geophysical terms, present the focus and goals of this research, and describe its place within current research needs in Green Bay.

Relevant previous research to hydrodynamics and sediment transport in Green Bay include studies on sediment resuspension and particle settling velocities (Eadie et al., 1991), measurement of horizontal sediment transport (Hawley & Niester, 1993), on patterns of mass sedimentation and of deposition of sediment contaminated by PCBs (Manchester-Neesvig et al., 1996), on sedimentary phosphorus (Klump et al., 1997), modeling hydrodynamics, sediment transport and sorbent dynamics (HydroQual Inc., 1999), on benthic carbon and nitrogen mass balances (Klump et al., 2009), explaining the role of circulation and heat fluxes in the formation of stratification leading to hypoxia in Green Bay (Hamidi et al., 2015), a biogeochemical analysis of hypoxia in Green Bay (Labuhn, 2017), analysis of the physical drivers of the circulation and thermal regime impacting seasonal hypoxia in the bay (Bravo et al., 2017), satellite-based estimations of surficial sediment transport (Hamidi et al., 2017), quantifying the influence of cold-water intrusions in Green Bay (Grunert et al., 2018), and estimation of transport timescales (Bravo et al., 2019). Previous relevant research done on Lake Michigan and the Laurentian Great Lakes watershed include studying influences of suspended sediments on the ecosystem in Lake Michigan (Chen et al., 2004; Ji et al., 2002), a 3D coupled bio-physical modeling experiment on the St. Clair River, Lake St. Clair, and Detroit River System (Anderson

et al., 2010), relationships between wind-driven and hydraulic flow in Lake St. Clair and the St. Clair River Delta (Anderson & Schwab, 2011), simulating a phytoplankton bloom in Lake Michigan using a coupled physical-biological model (Luo et al., 2012), predicting the oscillating bi-directional exchange flow in the Straits of Mackinac (Anderson & Schwab, 2013), modeling the climatology of seasonal general circulation and thermal structure in the Great Lakes (Bai et al., 2013), modeling the effect of invasive quagga mussels on the spring phytoplankton bloom in Lake Michigan (Rowe et al., 2015), investigating the thermal response to meteorological forcing in a hydrodynamic model of Lake Superior (Xue et al., 2015), modeling *Escherichia coli* at Beaches in Southern Lake Michigan (Safaie et al., 2016), modeling of dreissenid mussel impacts on Lake Michigan (Shen, 2016), modeling wind-waves from deep to shallow waters in Lake Michigan (Mao & Xia, 2017), biophysically modeling the influence of invasive quagga mussels, phosphorus loads, and climate on spatial and temporal patterns of productivity in Lake Michigan (Rowe et al., 2017), a study on the dynamics of wave-current-surge interactions in Lake Michigan (Mao & Xia, 2020), and an investigation of the drivers of warmings in deep-waters of Lake Michigan (Anderson et al., 2021).

There is vast research on marine estuaries, so we will just mention as examples the book Estuarine Ecohydrology by Wolanski & Elliott (2015), a study on the impact of tides and winds on estuarine circulation in the Pearl River Estuary (Lai et al., 2018), a study on the influence of suspended sediment front on nutrients and phytoplankton dynamics off the Changjiang Estuary (Ge et al., 2020), and an article on estuarine ecohydrology study of sediment transport in coastal zones by (Ouillon, 2018). Wolanski & Elliott (2015) defined an estuary as a semi-enclosed body of water connected to the sea as far as the tidal limit or the salt intrusion limit and receiving freshwater runoff, recognizing that the freshwater inflow may not be perennial (i.e., it may occur only for part of the year) and that the connection to the sea may be closed for part of the year (e.g., by a sand bar), and that the tidal influence may be negligible. Sediments determine the estuarine bed habitats (i.e., the fundamental niche for the fauna and flora on the bottom) and they influence organisms in the water column. Sediments are mobile and their dynamics occur at time scales of millennia, of intermediate timescales due to the tides, of storms, of river floods, of the seasons, and of turbulence.

The Green Bay estuary is a semi-enclosed body of water connected to the freshwater Lake Michigan as far as the limit of lake intrusion and receiving freshwater runoff. The

circulation, thermal regime, wave regime, and sediment transport in Lake Michigan and its Green Bay estuary are driven by the momentum flux generated by wind, the heat flux across the water surface, the Earth's rotation, thermal stratification, and topography (Bravo et al., 2017). While marine estuaries are subject to tidal influence and saltwater intrusion, in freshwater estuaries like Green Bay, the tidal influence is relatively smaller and salinity effects are nonexistent. The role of the large receiving and exchanging large body of water is played by lake water intrusion of currents, waves, and transport of waters with very different quality parameters such as density, temperature, and conductivity. Understanding the simultaneous effects of tributary flows and lake water intrusions is vital to comprehend the dynamics of freshwater estuaries.

Previous hydrodynamic and transport modeling of Green Bay was done either by employing nested models of the bay that represent the exchange of mass, energy, and momentum with Lake Michigan using potentially problematic open boundary conditions, generally obtained from low-resolution lake models (Hamidi et al., 2015; HydroQual Inc., 1999), or else using whole-lake models that lack the desired high resolution in the bay (Lee et al., 2005, 2007; Mao & Xia, 2017; Rowe et al., 2015; Rowe et al., 2017; Safaie et al., 2016; Shen, 2016). The study presented herein bypasses the use of open boundary conditions by developing a single hydrodynamic, wave, and sediment transport model of the lake that has high resolution in the bay and in the exchange zone between the open lake and the bay.

The purposes of this research were to: a) use the existing database of hydrodynamic, wave, and sediment field data to develop a predictive model of sediment transport in Lake Michigan, with an emphasis on Green Bay; b) use the sediment transport model to contribute to understanding ecological and environmental problems in the bay, and to recommend long-term solutions; and c) analyze summertime patterns of circulation, wave action, current and wave-induced bottom shear stress, thermal structure, and sediment transport in Lake Michigan, with special attention to Green Bay. The sediment transport model is designed to be a compatible component of the NOAA Lake Michigan-Huron Operational Forecast System (LMHOFS) for future water quality and shoreline protection applications for Lake Michigan and other Great Lakes.

Green Bay represents a true "proving ground" for adaptive restoration. Among the main recommendations of a recent summit on the "Ecological and Socio-Economic Tradeoffs of Restoration in the Green Bay Ecosystem" was the creation of a "Green Bay Ecosystem Simulation and Data Consortium" serving as a data clearing house, building upon the significant progress to date, and developing a modeling framework and visualization tools, furthering public outreach efforts, and ensuring a sustained growth in scientific expertise (Klump et al., 2018). Gaps in biogeochemistry and hydrodynamics identified during the restoration summit include incorporation of wind-wave models and an understanding of resuspension and its role in carbon and phosphorus cycling, the delineation of diagenetic vs. rapid carbon remineralization and its influence on sediment and water column respiration, the role of denitrification and nitrogen-fixation in the overall nitrogen budget for the bay and its link to nutrient stoichiometry and phytoplankton and cyanobacterial production. Extending models to multiple-year simulations, linking to refined watershed models, and engaging a complete range of downscaled regional climate scenarios to assess the magnitude of projected variability for the 21st century are necessary to provide more robust projections and guide expectations for adaptive management efforts (Klump et al., 2018). The present study addressed the incorporation of physical processes including wind-wave dynamics and sediment transport, will be used to extend models to multiple-year simulations, will engage downscaled regional climate scenarios to assess variability during the 21st century, and sets the stage for future work on other biogeochemical modeling gaps listed above.

2 Model Components and Formulation

Physically-based sediment transport modeling is essential in Green Bay due to complicated conditions of the system dynamics. Previous efforts intended to understand physical processes and particle dynamics in Green Bay faced obstacles in model development. Major obstacles included the use of Cartesian structured rectangular grids in POM-based models that limits the representation of small-scale shoreline features in Green Bay, and difficulties in modeling thermal structures and stratified flows in the shallow estuarine systems, especially during upwelling or downwelling events. Challenges in the implementation of Environmental Fluid Dynamics Code (EFDC) models were difficult documentation and neglected wind-wave

effects. Additionally, those models are computationally expensive and not very efficient if a high-resolution grid in a large domain such as Lake Michigan is implemented.

To overcome those obstacles, a state-of-the-art modeling approach, the Finite-Volume Community Ocean Model (FVCOM) was used in this research. FVCOM's features such as the use of an unstructured-grid solver and a parallel mode computation option make it a suitable candidate for the Green Bay sediment transport model. FVCOM is also equipped with several water quality tools that can integrate different physical and biogeochemical processes and enhance the implementation of transport models in restoration applications.

2.1 Circulation Model: FVCOM

Developed by Chen et al. (2003), FVCOM is a free-surface, primitive-equation ocean model and is a powerful numerical solution of the conservation of mass, momentum, and energy principles that solves for currents, temperature, salinity, density, and other hydrodynamic variables as follows:

$$\frac{\partial u}{\partial t} + u\frac{\partial u}{\partial x} + v\frac{\partial u}{\partial y} + w\frac{\partial u}{\partial z} - fv = -\frac{1}{\rho_W}\frac{\partial p}{\partial x} + \frac{\partial}{\partial z}\left(K_V\frac{\partial u}{\partial z}\right) + F_u \quad (1)$$

$$\frac{\partial v}{\partial t} + u\frac{\partial v}{\partial x} + v\frac{\partial v}{\partial y} + w\frac{\partial v}{\partial z} + fu = -\frac{1}{\rho_W}\frac{\partial p}{\partial x} + \frac{\partial}{\partial z}\left(K_V\frac{\partial v}{\partial z}\right) + F_v \quad (2)$$

$$\frac{\partial w}{\partial t} + u\frac{\partial w}{\partial x} + v\frac{\partial w}{\partial y} + w\frac{\partial w}{\partial z} = -\frac{1}{\rho_W}\frac{\partial p}{\partial x} + \frac{\partial}{\partial z}\left(K_V\frac{\partial w}{\partial z}\right) + F_w \quad (3)$$

$$\frac{\partial u}{\partial x} + \frac{\partial v}{\partial y} + \frac{\partial w}{\partial z} = 0 \quad (4)$$

$$\frac{\partial TW}{\partial t} + u\frac{\partial TW}{\partial x} + v\frac{\partial TW}{\partial y} + w\frac{\partial TW}{\partial z} = \frac{\partial}{\partial z}\left(K_H\frac{\partial TW}{\partial z}\right) + F_{TW} \quad (5)$$

$$\rho_W = \rho_W(TW, p) \quad (6)$$

where *(u, v, w)* are the components of the current in *(x, y, z)* Cartesian grid space, ρ_W is the water density, *p* is the pressure, *TW* is the water temperature, *f* is the Coriolis coefficient, K_V and K_H are the vertical eddy viscosity and thermal diffusion coefficients, and F_u, F_v, F_w, and F_{TW} represent the momentum and thermal diffusion terms. FVCOM uses a modified MY-Level 2.5

turbulence closure scheme (Mellor & Yamada, 1982) for vertical mixing calculations and Smagorinsky's (1963) eddy scheme for horizontal mixing.

FVCOM has several features that make it an efficient computational tool for the physical modeling of large lakes. FVCOM runs based on unstructured sigma-coordinated (terrain-following) grids, in which the 3D domain is discretized into triangular finite volumes. That feature increases model flexibility in representing irregular geometry of shorelines in the Green Bay estuary and preserves fine features of several peninsulas and islands that restrict physical processes in the bay. Additionally, FVCOM is computationally efficient because it runs in parallel and also adopts a split mode numerical scheme, in which it first calculates the water surface elevation and depth-averaged currents in the external mode and then solves for the vertical diffusive transport in a 3D internal mode.

FVCOM has been successfully implemented in various hydrodynamic applications such as coastal modeling (e.g., Chen et al., 2003, 2007; Huang et al., 2008; B. Li et al., 2017; J. Li et al., 2018; Zhang et al., 2018), Great Lakes studies (e.g., Anderson et al., 2010; Anderson & Schwab, 2011; Bai et al., 2013; Mao et al., 2016; Mao & Xia, 2020; Read et al., 2010; Shore, 2009; Xue et al., 2015), and modeling rivers, straits, and channels (e.g., Anderson & Phanikumar, 2011; Anderson & Schwab, 2013; Guerra et al., 2017; Lai et al., 2018). It has also been coupled with water quality and biogeochemical models in various case studies (e.g., Luo et al., 2012; Rowe et al., 2015; Rowe et al., 2017; Safaie et al., 2016; Shen, 2016). In this study, we used FVCOM version 4.1 to develop the physical circulation model of Lake Michigan.

2.2 Wave Model: FVCOM-SWAVE

Sediment movement is primarily due to advective-diffusive transport in the water column; however, sediment processes near the bottom are significantly affected by the wave interactions. Therefore, the implementation of wave actions in the sediment model is an important step toward simulations of more realistic current-wave-sediment interactions in the bottom boundary layer. Simulating WAves Nearshore (SWAN) model is adopted by FVCOM (FVCOM-SWAVE) as the wave simulator. SWAN was developed by Booij et al. (1999) and models wave evolution using transport equations to solve for wave action density N as follows:

$$\frac{\partial N}{\partial t}+\frac{\partial c_x N}{\partial x}+\frac{\partial c_y N}{\partial y}+\frac{\partial c_\sigma N}{\partial \sigma}+\frac{\partial c_\theta N}{\partial \theta}=\frac{S_w}{\sigma} \quad (7)$$

where N is the energy density E divided by the relative frequency σ, $N(\sigma,\theta)= E(\sigma,\theta)/ \sigma$, (c_x, c_y) are the propagation velocities in the (x, y) Cartesian grid coordinates, σ and θ are the intrinsic wave frequency and direction, c_σ is the propagation velocity due to variations in depth and currents, c_θ is the propagation in wave direction, and S_w is acting as a source/sink term to represent the effects of wind-wave generation, energy dissipation due to whitecapping, depth-induced wave breaking, and bottom friction, and nonlinear wave-wave interactions. Specific details of the SWAN model formulation and validation are described in the literature (Booij et al., 2004; Ris et al., 1999). SWAN is a structured-grid wave model and was converted to an unstructured-grid finite-volume model to be consistent with FVCOM (Chen et al., 2013; Qi et al., 2009).

SWAN has become popular in various applications including ocean wave simulations, engineering applications, modeling coastal and estuarine systems, and wave forecasting studies (Chen et al., 2018). SWAN is particularly adjusted for coastal regions with shallow waters, which makes it suitable for modeling sediment transport in Green Bay. Recent applications of the SWAN in studying Lake Michigan wave dynamics have also indicated good performance and applicability of the model for the Green Bay sediment transport studies (Mao et al., 2016; Mao & Xia, 2017).

2.3 Sediment Transport Model: FVCOM-SED

We used the FVCOM built-in sediment transport model (FVCOM-SED) in this study to model sediment processes in Green Bay and Lake Michigan. FVCOM-SED was developed based on the Community Sediment Transport Modeling Systems (CSTMS) by Warner et al. (2008) and was further modified to account for cohesive and mixed sediment dynamics (Sherwood et al., 2018). CSTMS was developed to be coupled with the structured-grid-based Regional Ocean Modeling System and was modified to be consistent with FVCOM unstructured-grid solver (Chen et al., 2013).

FVCOM-SED accounts for several sediment mechanisms including suspended and bedload transport, layered bed dynamics, and erosion/deposition actions for an unlimited number of cohesive and non-cohesive sediment classes. Each sediment class is characterized by mean

grain diameter, particle density, settling rates, and bed erosion characteristics. Each bed layer is defined based on the bulk characteristics of sediment classes in that layer and its initial thickness. The FVCOM-SED version 4.1 was only able to initiate the sediment transport model based on the uniform distribution of sediment classes in the entire domain. That seems to be an unrealistic assumption for Lake Michigan sediment stratigraphy. Therefore, we updated the code so that the model can take user-defined non-uniform distribution of sediment classes in the bed layer (Khazaei, 2020; Appendix A).

Bed layer characteristics, in particular thickness, is immediately affected by sediment actions such as erosion and deposition. In order to keep the number of bed layers constant throughout the simulation, an active layer is considered on top of sediment layers. The thickness of this active layer (z_a) is calculated in each time step based on the Harris and Wiberg's (2001) formulation as follows:

$$z_a = max\left[k_1(\tau_{sf} - \tau_{ce}),\quad 0\right] + k_2 D_{50} \qquad 8)$$

where τ_{sf} is the maximum bottom friction shear stress due to combined effects of currents and waves (N/m^2), τ_{ce} is the critical shear stress for erosion (N/m^2), D_{50} is the median grain diameter at the sediment-water interface (m), and k_1 and k_2 are empirical constants with values of 0.007 and 6.0, respectively. Sediment transport is limited to the mass available in the active layer in each time step.

The total load is the accumulated suspended load in the water column and bedload. FVCOM-SED calculates the suspended load by accounting for advective and diffusive concentration-based transport in the water column, as follows:

$$\frac{\partial C}{\partial t} + \frac{\partial uC}{\partial x} + \frac{\partial vC}{\partial y} + \frac{\partial wC}{\partial z} = \frac{\partial}{\partial x}\left(A_H \frac{\partial C}{\partial x}\right) + \frac{\partial}{\partial y}\left(A_H \frac{\partial C}{\partial y}\right) + \frac{\partial}{\partial z}\left(A_V \frac{\partial C}{\partial z}\right) + \frac{1}{H_z} C_{Source/sink} \qquad 9)$$

where C is the suspended sediment concentration, (u, v, w) are the three components of currents in the (x, y, z) Cartesian grid space, A_H and A_V are the horizontal and vertical eddy viscosity, and H_z is the thickness of grid cells. $C_{source/sink}$ accounts for additional vertical transport mechanisms due to settling and resuspension:

$$C_{source/sink} = -\frac{\partial \omega C}{\partial S} + E_s \qquad 10)$$

where ω is the settling velocity positive in the upwards direction (*m/s*) and E_s is the erosion rate ($kg/m^2/s$) in the vertical sigma coordinate direction *S*. Ariathurai and Arulanandan (1978) defined erosion rates of cohesive soils as a function of bed erodibility constant, sediment porosity (top layer sediment particles in this case), maximum bottom shear stress, and critical shear stress for erosion. Transport of suspended load is constrained to a zero-flux boundary condition at the surface of the water column and the net balance between erosion and deposition at the bottom.

While the suspended load includes the flux of sediment mass at the sediment-water interface and transport in the water column, the bedload is considered as the horizontal exchange within the top layer of the bed and is estimated based on the Hans Albert Einstein's definition of non-dimensional volumetric sediment flux:

$$q_{bl} = q_{s*} D_{50} \sqrt{(s-1) g D_{50}} \quad (11)$$

where q_{bl} is the horizontal bedload transport rate (m^2/s) and $s = \rho_s/\rho_w$ is the specific density of sediments in the water. q_{s*} is the magnitude of the non-dimensional transport rate and could be determined based on the Meyer-Peter and Müller's (1948) scheme.

Mixed-sediment bed processes occur when both cohesive and non-cohesive sediments are present and there is a considerable amount of mud (fine cohesive sediment) in the sediment layer (Mitchener & Torfs, 1996). FVCOM-SED (and CSTMS) adopts a method similar to Le Hir et al. (2011) and Mengual et al. (2017) to force resuspensions, in which mixed beds form when a mud content of 3 to 30% is present in the sediment layer. Their strategy is tested and recommended for implementation in real case 3D hydro-sedimentary modeling applications. This approach means that in mixed-sediment bed conditions effective critical shear stress of the bottom ($\tau_{ce,eff}$) is calculated based on a weighted combination of critical shear stresses of cohesive and non-cohesive portions of the bed:

$$\tau_{ce,eff} = max[P_c \tau_{cb} + (1 - P_c)\tau_{ce}, \tau_{ce}] \quad (12)$$

where τ_{ce} is the critical shear stress for each sediment class, τ_{cb} is the bulk critical shear stress for the sediment layer based on Sanford's (2008) approach, and P_c is the dimensionless cohesive behavior parameter. P_c is a function of the mud content in the bed layer with lower

values denoting a non-cohesive behavior and vice versa. It is important to note that while the bed erodibility of non-cohesive sediment is treated as the property of individual sediment classes, the erodibility of cohesive sediment is treated as the bulk property of the bed. Following Sherwood et al. (2018), the equilibrium bulk critical shear stress $\tau_{cb,eq}$ is defined in terms of an exponential profile defined by a slope and offset:

$$\tau_{cb,eq} = a\, e\exp\left[\frac{\ln\left(z_p\right) - \text{offset}}{\text{slope}}\right] \tag{13}$$

where z_p is mass depth defined as the cumulative dry mass of sediment overlying a given depth in the bed *(kg/m^2)* and a = 1 *Pa m^2/kg* is a dummy coefficient that produces the correct units of critical shear stress. The parameter values of *offset* = 2 *ln(kg/m^2)*, *slope* = 5 *ln(kg/m^2)*, and timescale for consolidation T_c = 8 *hours* were based on the recommendations of the CSTMS and FVCOM-SED settings.

FVCOM-SED is fully coupled with the FVCOM ocean model and FVCOM-SWAVE to account for the current-wave-sediment interactions (Chen et al., 2013). More details of the CSTMS model, mixed sediment transport mechanisms, and model validation are provided in the literature (Sherwood et al., 2018; Warner et al., 2008). In section 3.3, we elaborate on the characterization of different sediment classes and their properties for the Lake Michigan sediment transport model.

3 Model Design

3.1 Study Area

While the focus of the current study is Green Bay, to avoid the uncertainty and difficulty of obtaining internal or open-lake boundary conditions at the connection straits with Lake Michigan, a whole-lake model is developed. Green Bay is 190 *km* long in its longest axis and, on average, is about 20 *km* wide. With an average and maximum depths of approximately 20 *m* and 50 *m*, respectively, Green Bay is considered a shallow coastal water body. The maximum depth in Lake Michigan is about 280 *m*.

Chambers Island cross-section divides Green Bay into lower and upper sections. Lower Green Bay is the hotspot of environmental issues, where Fox River discharges runoff from the heavily developed and stressed Fox River watershed into the bay. The watershed is mostly

covered by vegetated areas (Khazaei & Wu, 2018), and the cities of Appleton and Green Bay, large industrial sites, and farmlands impact the concentration and quality of particles running into the river (Klump et al., 1997; Velleux et al., 1995). The Fox River alone contributes about two-thirds of the nutrient and particulate tributary loading into Green Bay and almost one-third of the total phosphorus load to Lake Michigan (Harris & Christie, 1987). Figure 1 shows the location of Lake Michigan and Green Bay in the Great Lakes basin and Green Bay AOC.

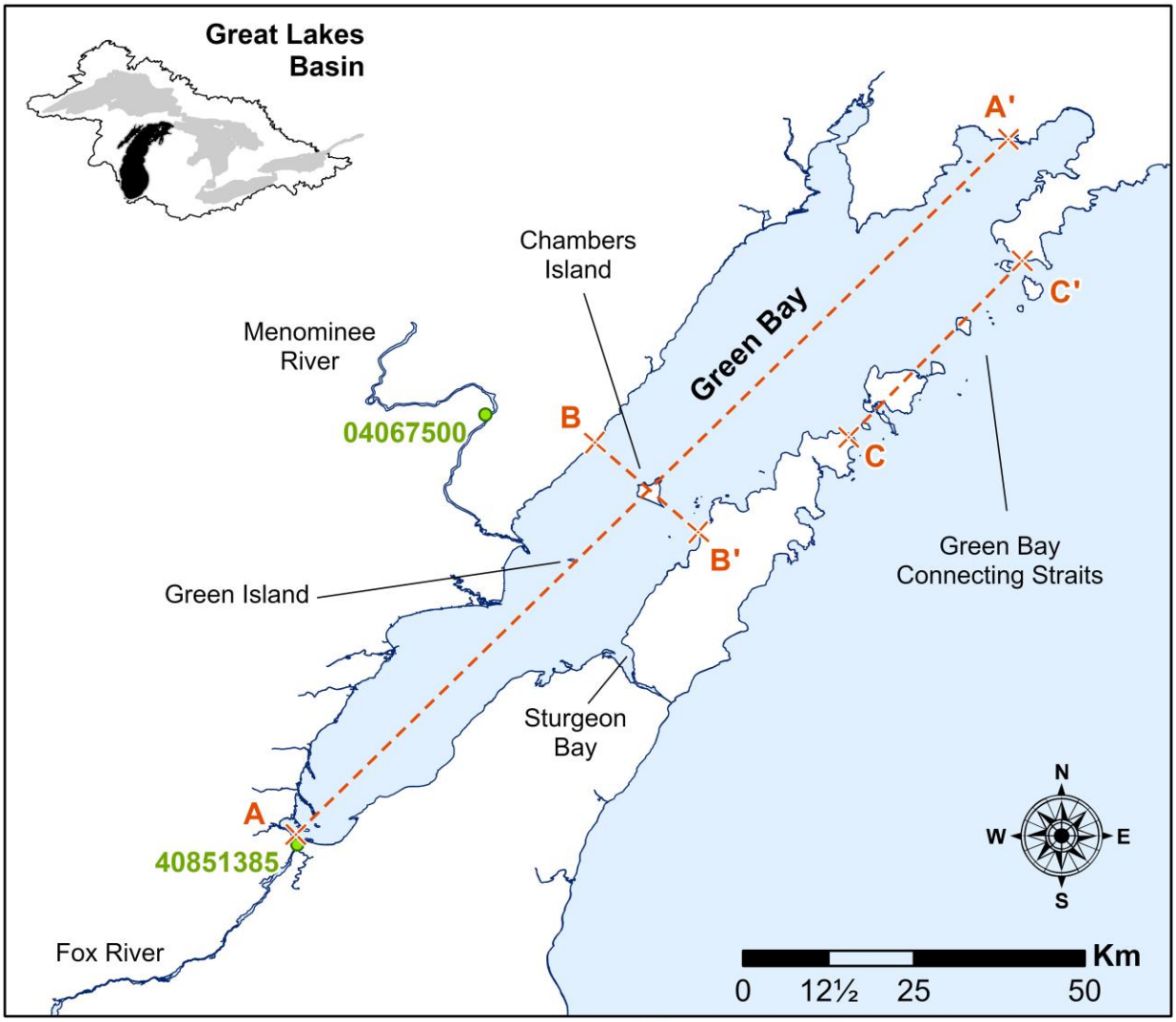

Station Name	Station ID	Lat	Lon
Southern Green Bay Buoy	45014	44.80	-87.76
Milwaukee Atwater 20m Buoy	45013	43.10	-87.85
Northern Michigan Buoy	45002	45.34	-86.41
Southern Michigan Buoy	45007	42.67	-87.03
Sleeping Bear Dunes Buoy	45183	44.98	-85.83
Green Bay West Buoy	GBW	44.58	-87.99
Green Bay East Buoy	GBE	44.55	-87.96
NEW Water Station 13	NW13	44.53	-88.01
USGS Fox River Gauge	40851385	44.53	-88.01
USGS Menominee River Gauge	04067500	45.33	-87.66
USGS Lake Michigan at Gary	04092788	41.65	-87.43
USGS Lake Michigan at Hyde Park	04092440	41.78	-87.57

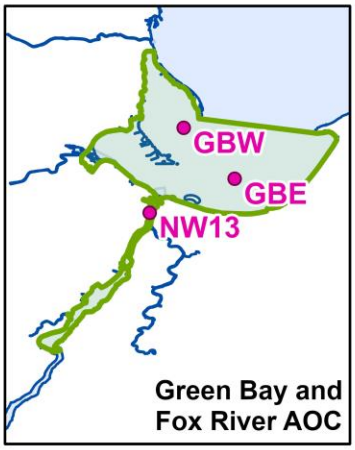

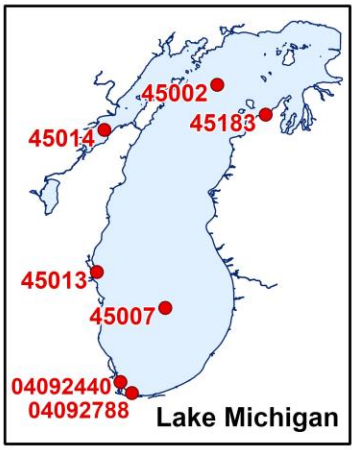

Figure 1. Green Bay Location in Lake Michigan and the Great Lakes basin. Lower insets show Lake Michigan and the Green Bay Area of Concern (AOC). Buoy stations and USGS gauges used in this study and their abbreviations are also shown in the Figure. Cross-sections A-A', B-B', and C-C' are used to look at transport patterns in different locations across the bay.

3.2 Grid and Simulation Specifications

Circulation and transport mechanisms are very sensitive to the morphology of the system. Shallow waters and the complex geometry of the Green Bay shorelines require a fine grid that can resolve those detailed features (Figure S1 in the Supporting Information). Long Tail Point and Little Tail Point Islands located on the western shore of lower Green Bay, Green and Chambers Islands in the central bay areas, as well as Plum, Detroit, Washington, Rock, St. Martin, Poverty, Summer, and Little Summer Islands in the exchange zone of the Lake Michigan and Green Bay were incorporated in the grid (see Figure S2 in the Supporting Information). Also, the coastline data was updated to include the Cat Island, a feature that is crucial in modeling the circulation and transport in the Green Bay AOC.

Bathymetry and shoreline data, used to generate the Lake Michigan unstructured grid (Figure S3 in the Supporting Information), are based on NOAA datasets (National Geophysical Data Center, 2015; NOAA, 2017) and were updated in the southern Green Bay to represent recent changes of the bathymetry due to the dredging of navigational channel project.

The Lake Michigan grid in this study includes 52,574 triangular elements/cells, 28,985 nodes, and is vertically discretized to 20 σ-layers, i.e., layers follow terrain variations. The grid is designed very dense in Green Bay, where element side length varies between 50 *m* to 1500 *m* from the mouth of Fox River to upper Green Bay. Since the focus of our model is to simulate sediment transport in Green Bay, a coarser grid resolution is used for the main body of Lake Michigan for the sake of computational efficiency. Given the suggested summertime baroclinic Rossby radius of 5 *km* in the Great Lakes, it is critical to use a grid size less than 5 *km* within the 8-10 *km* of the coastal areas (Beletsky et al., 1997, 2006b). Therefore, cell side length in the Lake Michigan grid was designed to vary between 1000 *m* in the shorelines to about an average of 5 *km* in the central lake areas. A relatively fine grid is constructed near the connecting straits to be able to accurately account for the exchanges between the lake and the bay.

FVCOM-SWAVE offers various options suitable for the simulation of waves in different physical conditions (Booij et al., 1999; Table 1). In this study, the wave model was adjusted by selecting from those options based on recommendations in the literature (Mao et al., 2016; Ris et al., 1999), and our comparisons of simulated results against the validation buoys in nearshore and deep-water areas of Lake Michigan. In this regard, the third generation of the SWAN wave

363 model (Booij et al., 1999) with quadruplet wave-wave interactions of Hasselmann et al.'s (1985)
364 was adopted for this study. We also used Komen et al.'s (1984) formulation for wind growth and
365 whitecapping, Hasselmann et al.'s (1973) expressions for bottom friction, and Battjes & Janssen's
366 (1978) formulation for depth-induced breaking calculations. We also selected 60 as the number
367 of steps in the relative frequency space.

368 **3.3 Sediment Classification and Properties**

369 Sediment transport models require a set of standard parameters for model simulations,
370 which can be obtained through observations, lab experiments, and/or calibration. Those
371 important parameters include particle density (ρ_s), mean diameter (D_{50}), and porosity (φ).
372 Prediction of sediment transport is also very sensitive to erosion and deposition characteristics of
373 the particles such as critical shear stress for erosion (τ_{ce}) and settling rates (ω). A previous Lake
374 Michigan sediment transport model has found ~40% deviations in results by changing these
375 parameters (Lee et al., 2005), yet, the model had the most sensitivity to the fraction of fine-
376 grained particles in the sediment mixture. Therefore, it is important in the first place to define the
377 distribution of sediment classes in the bed layer.

378 We extracted information from several studies to obtain a general understanding and
379 reasonable estimates of sediment characteristics in Green Bay. The next steps included using soil
380 classification methods/standards and consultation with experts to narrow down the ranges
381 defined for each parameter in the literature. Finally, some of these model parameters were
382 adjusted based on model calibration.

383 There are few studies of Green Bay sediment classes and their distribution. Field
384 observations and analysis of sediment samples (HydroQual Inc., 1999; Jones, 2000; Moore et al.,
385 1973; Wisconsin DNR, 2000) have found clay, silt, and sand are the major constituting variables
386 of lower Green Bay. As we move from south, near the mouth of Fox River, to the north, near the
387 connecting straits, mud content decreases in the bed layer and the upper Green Bay bed is mostly
388 formed by sand and gravel. We compiled these findings with Lee et al.'s (2007)
389 recommendations for Lake Michigan and estimated bottom sediment stratigraphy as shown in
390 Figure S4 in the Supporting Information. These patterns are also consistent with distributions of
391 cohesive sediment in Green Bay (HydroQual Inc., 1999). It is important to mention that the
392 composition of the benthic zone in Lake Michigan has changed due to the invasion of Zebra and

Quagga Mussels. Zebra mussels were first observed in Green Bay in 1991 and Quaggas in 2003. In lower Green Bay and the inner bay, the distribution of dreissenid mussels is patchy (Qualls et al., 2013) and in the depositional areas of the bay they are absent. This is almost certainly due to recurring summertime hypoxia in the mid and lower bay (Kaster et al., 2018; Klump et al., 2018). Hypoxic events have also been repeatedly observed from time series dissolved oxygen sensors deployed recently in the shallow waters of the inner bay. The influence of dreissenids on sediment resuspension is difficult to judge with certainty, but would appear minor relative to physical processes. Those changes are neglected in the assignment of bottom sediment initial conditions, yet have to be considered in future studies for improved simulations of sediment transport when sufficient information becomes available (see Figure S5 in the Supporting Information).

We identified six sediment classes for the current model development and determined sediment mean diameter based on the U.S. Department of Agriculture (USDA) soil classification standard (Yolcubal et al., 2004) as shown in Table 1. Density and porosity of different sediment classes were also estimated based on the analysis of sediment samples taken in Green Bay (Manchester-Neesvig et al., 1996; Wisconsin DNR, 2000).

Table 1. Sediment properties and erosion/deposition characteristics used in the Lake Michigan sediment transport model.

Sediment class	**1**	**2**	**3**	**4**	**5**	**6**	**Source**
Sediment type	Clay	Fine Silt	Coarse Silt	Fine Sand	Coarse Sand	Gravel	Moore et al. (1973), Wisconsin DNR (2000), and Lee et al. (2007)
D_{50} **(mm)**	0.001	0.008	0.05	0.1	0.5	2	Jones (2000) and Yolcubal et al. (2014)
ρ_s **(kg/m^3)**	2300	2300	2300	2450	2450	2450	Wisconsin DNR (2000)
Φ **(%)**	97.5	97.5	97.5	85	75	60	Manchester-Neesvig et al. (1996)
ω **(mm/s)**	0.001	0.02	1.01	4.95	57.04	175.31	Garcia (2008)
τ_{ce} **(N/m^2)**	0.008	0.029	0.09	0.18	0.25	1.10	Garcia (2008)
E_0 **(kg/m^2/s)**	0.0005	0.0025	0.005	0.005	0.005	0.005	Ariathurai and Arulanandan (1978)

Previous studies have shown wide ranges of sediment settling/fall velocity in Green Bay. NOAA sediment trap study found settling velocities of about 6-70 *mm/s* in stratified conditions (summertime) and 14-200 *mm/s* during unstratified periods. We used a method proposed by Soulsby (1998) that estimates fall velocity based on sediment mean diameter and density and viscosity of water. This method is suitable for fine-grained sediments, therefore, we used for coarser sediment classes a graphical method explained by García (2008, p. 42), which requires the same variables as Soulsby's method.

While settling velocity governs deposition, bottom erosion and resuspension events are controlled by critical shear stress for erosion which we estimated based on the definition of Shields non-dimensional critical shear stress (τ_c^*). τ_c^* can be found based on the modified Shields diagram (Parker, 2004) or alternatively for finer particles based on Mantz's (1977) empirical relationship. Critical shear stress for erosion is then a function of τ_c^*, particle density, and mean sediment diameter according to the Shields formulation.

FVCOM-SED requires a bed erodibility constant (E_0) in order to estimate bottom sediment fluxes. A wide range of values is suggested in the literature for E_0. Ariathurai and Arulanandan (1978) conducted several tests on more than 200 natural or lab-synthesized fine and cohesive sediment samples and suggested values between 5×10^{-4} and 5×10^{-3} $kg/m^2/s$. Analysis of those samples has shown that the slope of erosion rate curves increases proportionally to critical shear stress for erosion.

3.4 River Inputs

Tributary loadings are the major input fluxes into Green Bay. Required river inputs for the circulation, wave, and sediment transport models are discharge, temperature, and total suspended solids (*TSS*) at river mouth that were estimated in this study based on daily USGS observational data. USGS observations during the 2011-2019 period show average inflowing discharge of 170, 24, 29, and 106 m^3/s and *TSS* concentrations of 24, 0.24, 0.03, and 3 *mg/L* for the Fox, Oconto, Peshtigo, and Menominee Rivers, respectively. Those statistics indicate that the Fox and Menominee Rivers have more influence on circulation and thermal regimes in Green Bay, hence they were included as boundary conditions of the model.

It should be noted that riverine *TSS* loading into the bay is estimated based on empirical relationships developed using USGS observations of discharge and turbidity at the mouth of Fox River (gage ID: 40851385) and cruise measurements of turbidity and *TSS* by the city of Green Bay Sewerage district, now NEW Water, at this location (Khazaei, 2020; Khazaei et al., 2018; NEW Water, 2017). The Fox River sediment load composition varies by flowrate. For the regular summertime flowrates in the Fox River (less than ~300 m^3/s), observations by Jones (2000) show that ~50% of Fox River sediments are very fine materials with mean diameter size less than 0.005 *mm*, ~40% are materials with a mean dimeter of 0.05 *mm*, and ~10% are coarser materials. Therefore, we assumed 50% Clay, 35% Fine Silt, 10% Coarse Silt, 3% Fine Sand, and 2% Coarse Sand in the incoming river loads.

3.5 Field Data

Previous efforts in modeling physical and biogeochemical processes in Green Bay have been challenged by the scarcity of relevant hydrodynamic and water quality observational data. Recent data collection efforts, such as continuous monitoring of turbidity at Green Bay West and East buoys in the southern bay (Miller, 2020), have made the development and validation of a sediment transport model for Green Bay possible. As explained above, we used NEW Water turbidity and *TSS* cruise data to convert turbidity observations into *TSS* time series. In addition, seven buoy stations in Lake Michigan and Green Bay were used to validate hydrodynamic and wave models, i.e., southern Green Bay, Atwater Beach in Milwaukee nearshore zone, Sleeping Bear Dunes, North Michigan, and South Michigan buoys (see Figure 1).

External forcing inputs of the model are based on the interpolation of NOAA National Centers for Environmental Information (NCEI; NOAA, 2018) land-based and buoy stations in the Great Lakes basin. The interpolation scheme is based on a natural neighbor method developed by NOAA Great Lakes Environmental Research Laboratory for application in the Great Lakes forecasting models (Beletsky et al., 2003; Schwab & Beletsky, 1998) and accounts for adjustments of overland to overlake conditions whenever data from land-base stations were used (Beletsky & Schwab, 2001).

3.6 Model Skill Criteria

We use Root Mean Squared Error (*RMSE*), Bias Deviation (*BD*), and correlation coefficients (*CC*) to assess model skills of scalar variables (e.g., temperature and *TSS*):

$$RMSE = \frac{1}{N}\left(\sum_{i=1}^{N}(e_i^2)\right)^{1/2} \quad (14)$$

$$BD = \frac{1}{N}\sum_{i=1}^{N}(e_i) \quad (15)$$

$$CC = \frac{\sum_{i=1}^{N}(x_{i,O} - x_{ave,O})(x_{i,P} - x_{ave,P})}{\left[\sum_{i=1}^{N}(x_{i,O} - x_{ave,O})^2\right]^{1/2}\left[\sum_{i=1}^{N}(x_{i,P} - x_{ave,P})^2\right]^{1/2}} \quad (16)$$

where N is the number of observation/prediction points, e_i is the deviation of the predictions from observations (i.e., $e_i = x_{i,O}\text{-}x_{i,P}$; where $x_{i,O}$ and $x_{i,P}$ are observational and prediction values at point i, respectively), and $x_{ave,o}$ and $x_{ave,P}$ are the mean of observed and predicted data, respectively.

To assess model skills for vector fields (e.g., currents) we use normalized Fourier norm (F_n) and average angular difference ($\Delta\theta$):

$$F_n = \frac{\|V_o, V_p\|}{\|V_0, 0\|} = \frac{\left(\frac{1}{N}\sum_{i=1}^{N}|V_{i,o} - V_{i,p}|^2\right)^{1/2}}{\left(\frac{1}{N}\sum_{i=1}^{N}|V_{i,o} - 0|^2\right)^{1/2}} \quad (17)$$

$$\Delta\theta = \frac{1}{\pi N}\sum_{i=1}^{N}\cos^{-1}\left(\frac{V_o . V_p}{|V_o||V_p|}\right) \quad (18)$$

where $V_{i,o}$ and $V_{i,p}$ denote observed and predicted vector fields at point i, respectively.

RMSE is used to assess model accuracy, i.e., zero indicates perfect model accuracy and as the value increases, model accuracy decreases. *BD* shows model bias and smaller values close to zero denote lower biased performance of the model. *CC* can be used as an indicator of model performance in reproducing the temporal patterns of change in observational data. In this article, *CC* is reported if significant at p-value ≤ 0.05. *Fn* and $\Delta\theta$ assess model accuracy in the prediction of vector fields magnitude and direction, respectively. F_n and $\Delta\theta$ equal to zero indicate a perfect model, values between zero and one are in the acceptable range, and as the value increases, model performance decreases.

4 Simulation Details and Model Validation

We ran the model for the 2016-2019 years and model simulations were limited to the May-October period of each year to focus on the ice-free period in Lake Michigan and time of active bottom layer sediment dynamics. Model stability requires simulations at a time step of 5 *s*. The circulation model is initiated at rest, i.e., zero currents. 3D temperature fields are interpolated from LMHOFS simulation in Lake Michigan at the initial condition. Also, the model is run using realistic initial water surface elevation in Lake Michigan (NOAA, 2020). We ignored major open boundary conditions around Lake Michigan, e.g., bi-directional flow at the Straits of Mackinac and Chicago River diversion, because they do not have an immediate impact on sediment transport in Green Bay, especially southern areas in the bay.

The bed layer and bottom sediment distribution are initialized in each year based on the non-uniform distribution of different sediment classes defined in section 3.3 (see Figure S4 in Supporting Information). Considering the average bottom distribution over the entire lake, the portion of cohesive (Clay, Fine Silt, and Coarse Silt) and non-cohesive (Fine Sand, Coarse Sand, and Gravel) sediment classes contributing to the bottom layer are 29% and 71%, respectively, i.e., cohesive sediments are defined as the mixture of clay and silt (Wolanski, 2007). Analysis of sediment samples in Green Bay showed that the average cohesive sediment depth in Green Bay is ~0.5 *m* (Wisconsin DNR, 2000). Average erosion and deposition patterns in Green Bay, as well as Lake Michigan (Lou et al., 2000), showed that bed changes do not exceed that value during long-term simulations of semi-annual to annual scales. Therefore, we started the model with a bed thickness of 0.5 *m*. We also conducted a sensitivity analysis of *TSS* simulations at GBE and GBW and found that although results are slightly sensitive to initial bed thickness, values in the range 0.25 *m* and 0.5 *m* result in a reasonable estimation of *TSS* simulations in Green Bay.

4.1 Validation of Simulated Currents, Waves, and Temperature Fields

Currents are the main driver of transport mechanisms in hydrodynamic simulations. Accurate simulations of sediment transport dynamics rely on accurate simulations of currents near the bottom. Figure 2 compares the observed and predicted daily currents in N-S (*v* component) and E-W (*u* component) directions during the May-October of 2016-2019 years. Comparison plots and model skill criteria indicate reasonable agreement between model and

buoy observations at two selected locations, given the complex nature of the physical process and the system. Our calculated model skill statistics for currents (or velocity fields) are comparable and in some cases show slight improvements compared with previous Lake Michigan hydrodynamic modeling efforts. For example, *Fn* values of 0.79-1.01 and 0.9-1.05 were reported respectively for barotropic (Schwab, 1983) and POM-based (Beletsky & Schwab, 2001) models of summertime circulation in Lake Michigan built on 5-*km* resolution grids. Rowe et al. (2015) obtained improved performance in modeling summertime hydrodynamics by using interpolated forcing and adopting FVCOM, and reported *Fn* values of 0.83-0.91. Schwab (1983) and Rowe et al. (2015) have respectively reported values of 0.23-0.46 and 0.29-0.31 for $\Delta\theta$ in modeling Lake Michigan currents direction. Wave action complements currents to force sediment movement. Combined current-wave action produces stronger shear stresses at the water-sediment interface and triggers more frequent and/or stronger episodes of resuspension. Hence, an accurate wave model will improve the understanding of sediment processes.

Figure 2 shows the comparison of observed and predicted significant wave heights (W_{Hs}) and wave directions (W_{dir}). W_{Hs} is defined as the average of the highest one-third of the waves, measured between wave trough to crest. According to the figure and model skill statistics, FVCOM-SWAVE simulations of wave height are in good agreement with observations at three selected buoys. In particular, high correlations between observations and simulations implies that patterns of the wave height variability are reproduced well by the model. However, wave direction predictions are not as accurate as wave heights. Comparison of the model skill statistics with previous wave models of Lake Michigan (Hawley et al., 2004; Mao et al., 2016) also suggests a good (in some cases improved) performance by the FVCOM-SWAVE model and its suitability for applications in modeling sediment transport.

We also validate predictions of temperature fields to assess the performance of the physical model in simulating circulation and transport. Also, temperature governs biogeochemical processes in the lake and is important for Green Bay restoration studies. As shown in Figure 2, the temperature is predicted with high accuracy at four selected buoys, except for over-estimation of mid-range bottom temperature at the location of Green Bay buoy station 45014. One possible explanation for that is the model's inability to fully capture cold water intrusion from Lake Michigan into the southern bay. Denser cold water from the lake flows near the bottom while warmer water, coming into the bay from rivers, flows on top; forming a two-

546 layered flow condition in Green Bay (Grunert et al., 2018). Yet, high correlations between
547 predicted and observed water temperature at this location, as well as other buoys, shows that the
548 model is capable of producing the patterns of variability in temperature profiles such as
549 upwelling events.

550

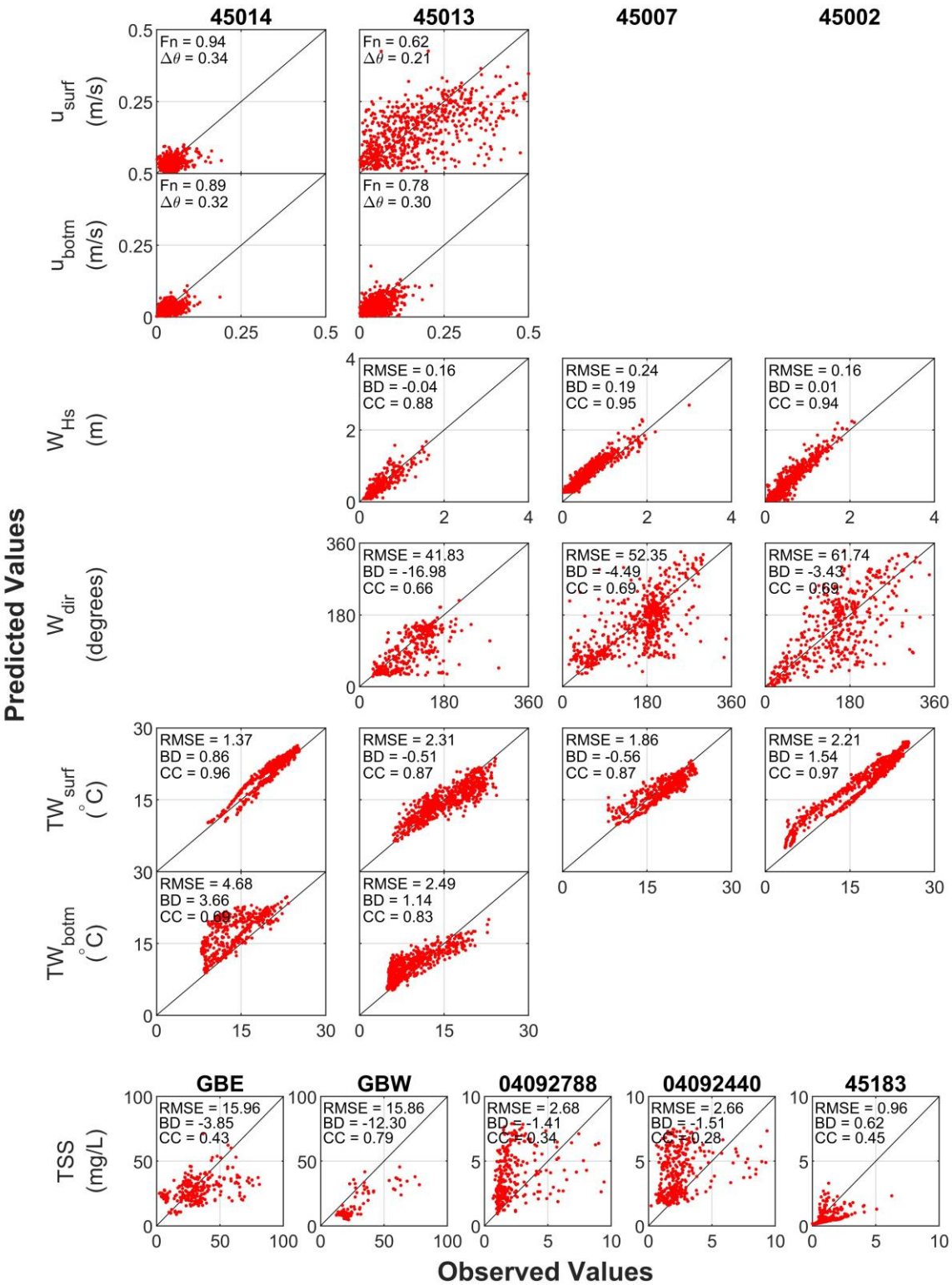

Figure 2. Comparison of the daily observed and predicted surface and bottom currents (u_{surf} and u_{botm}), significant wave height (W_{Hs}) and direction (W_{dir}), surface and bottom temperature (TW_{surf} and TW_{botm}), and total suspended solids (TSS) at the location of selected validation buoys during 2016-2019 years. Buoy locations are shown in Figure 1. CCs are reported if significant at P-value ≤ 0.05.

4.2 Validation of Simulated Total Suspended Solids

Figure 2 compares predicted daily *TSS* against the observations at five different locations in Green Bay and Lake Michigan, where turbidity observations are available in 2016-2019. Turbidity times series obtained at those locations were converted into *TSS* concentration using *TSS*-turbidity empirical functions for the estimation of river loadings (explained in section 3.4). GBW and GBE buoys are located in very shallow areas of lower Green Bay (~1 *m* depth) and sensor probes were placed at the mid-depth water column; therefore, observations represent the bottom sediment conditions. USGS 04092788 and 04092440 buoys are located in southern and southwestern Lake Michigan where multiple episodes of sediment resuspension events occur during the May-October period. Great Lakes Observing System (GLOS) 45183 buoy is located at Sleeping Bear Dunes in northeastern Lake Michigan with complex geomorphological characteristics of the lake that complicates sediment dynamics. 04092788, 04092440, and 45183 buoy stations represent surface conditions.

Figure 2 implies a fairly good accuracy and overall satisfactory performance of the model in modeling sediment transport in Green Bay AOC, given the physical complexity of the system. Although the model is biased at GBW buoy, high correlations between observed and predicted *TSS* values at GBW denotes model capability in the simulation of storm events and episodes of resuspensions. Figure S6 of the Supporting Information illustrates examples of resuspension events captured by the model at these two locations. In some cases, the model significantly underestimated *TSS* observations at both buoys. Those underestimations may be explained by sensor malfunction and/or sudden spikes of *TSS* concentrations due to construction activities near the GBW buoy (e.g., Cat Island project), dredging of Fox River, and navigation channel project.

Although the sediment model is focused on Green Bay, *TSS* validations at southern Lake Michigan (04092788 and 04092440 buoys) and Sleeping Bear Dunes (45183 buoy) are fairly satisfactory (Figure 2). Supplementary Figure S6 also shows that the model is able to produce the patterns of high-turbidity episodes in these distinct locations in southern and northern basins of Lake Michigan, although the magnitude of high resuspension events is not completely accurate.

Figure 3 also compares the surface snapshots of *TSS* concentration based on FVCOM simulations and MODIS imagery for six selected days in 2018. MODIS-based *TSS* maps are estimated based on a procedure explained in Hamidi et al. (2017), using relationships developed

between simultaneous surface reflectance and NEW Water *TSS* observations at the location of monitoring stations in lower Green Bay. We used MODIS product *MYD09GA* for the estimation of surface *TSS*. We picked several days during the summer of 2018 by visual inspection, and then used *MYD09GA Surface Reflectance 500m Quality Assurance* and *1km Reflectance Data State QA* layers to filter high-quality and cloud-free data. True-color visualization of raw imagery data is presented in Figure S7 of Supporting Information. Except for small deviations in August that could be explained by inaccurate estimation of *TSS* inputs and/or wind conditions, the model-simulated spatiotemporal patterns of *TSS* in lower Green Bay and decreasing gradient of suspended particles from Green Bay AOC towards Chambers Island match very well with the results of the remote sensing method.

Besides these point and spatial validations of the model's ability to predict *TSS*, we compared observed and predicted *TSS* profiles in lower Green Bay (45014 buoy) in 2018 to assess model skills in the simulation of vertical sediment profiles (Figure 4). Observational *TSS* profiles were inferred from the acoustic backscattering signal collected by *Nortek Aquadopp 600 kHz* Acoustic Doppler current profilers (ADCP) at 10 depth layers (GLOS, 2021). Backscattering signal was converted from echo intensity based on a procedure explained and used in previous studies (Deines, 1999; Lee et al., 2007). The backscattering signal was paired with turbidity data from a deployment at the Green Bay buoy station 45014 in July 2016. Turbidity data were collected by a *WET Labs NTUSB* turbidity sensor and were used to build relationships between turbidity and ADCP backscattering signal. Those relationships are used to estimate turbidity profiles, which were converted to *TSS* concentration profiles based on the empirical *TSS*-turbidity functions explained in section 3.4.

Figure 4 shows that the predicted *TSS* profiles resemble the patterns of the observed profiles and indicate the simultaneous occurrence of high-turbidity events, although the magnitude of *TSS* concentration deviates slightly during storm events. Comparison of the depth-averaged observed and predicted *TSS* profiles results in *RMSE*, *BD*, and *CC* skill metrics of 1.31 *mg/L*, -0.83 *mg/L*, and 0.47 at the Green Bay buoy station 45014. These model performance metrics show that the model is skillful in the simulation of *TSS* along the water column.

The array of validation methods used, including point validations of predicted *TSS* concentration, assessment of model performance during the high-turbidity events, comparison of

616 the surface *TSS* patterns with satellite imagery data, and validation of model's capability in
617 reproducing the *TSS* profiles indicate a reasonable accuracy of the physical sediment transport
618 model. As we will discuss with more details in the next sections, our results also agree with the
619 findings of previous studies and qualitatively matches the patterns of the bottom shear stress
620 forces and sediment transport in Lake Michigan (Lee et al., 2005, 2007; Lou et al., 2000).

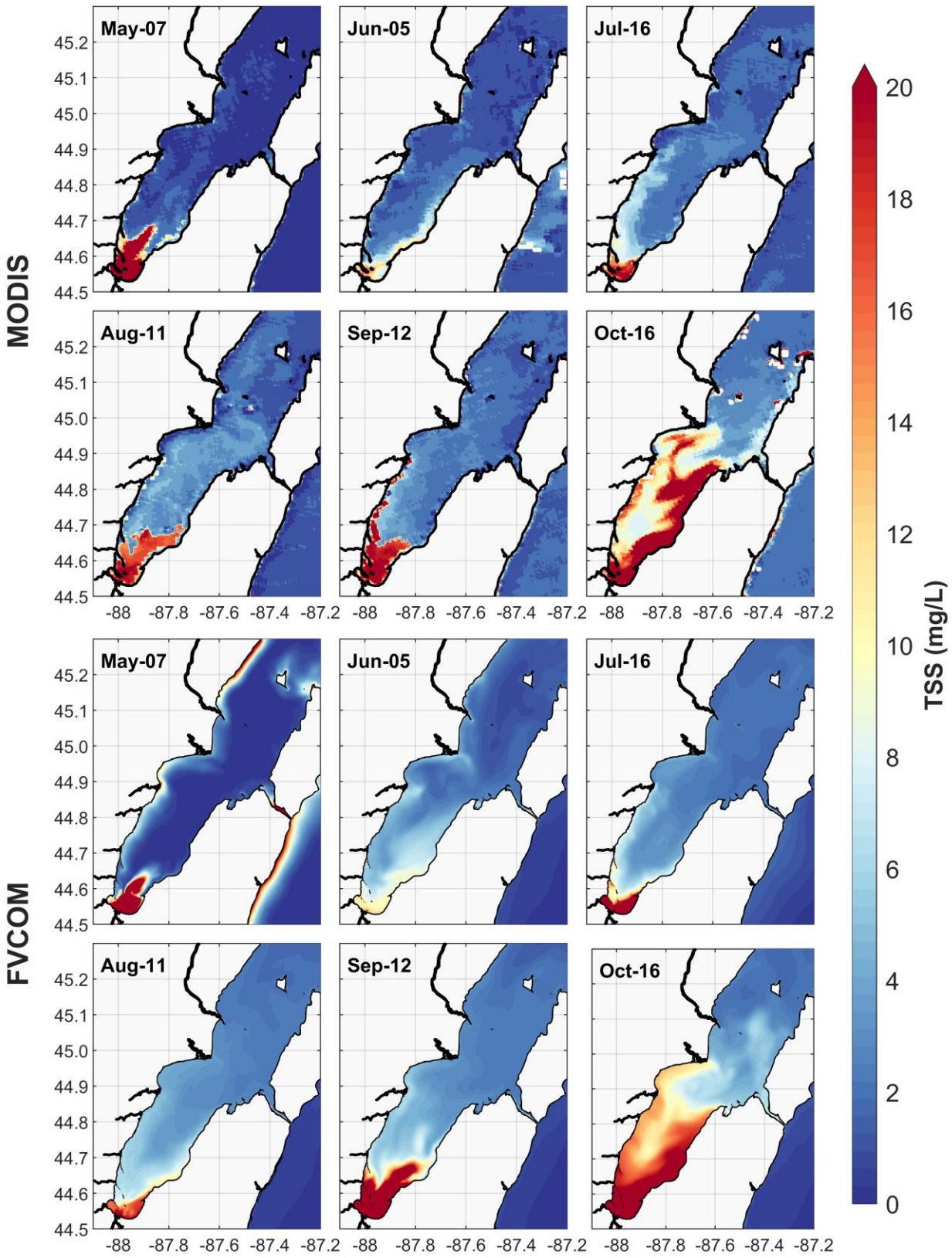

Figure 3. Snapshots of the surface total suspended solids (TSS) in Green Bay for six cloud-free selected days in May-October 2018 period based on MODIS imagery (top) and FVCOM simulations (bottom).

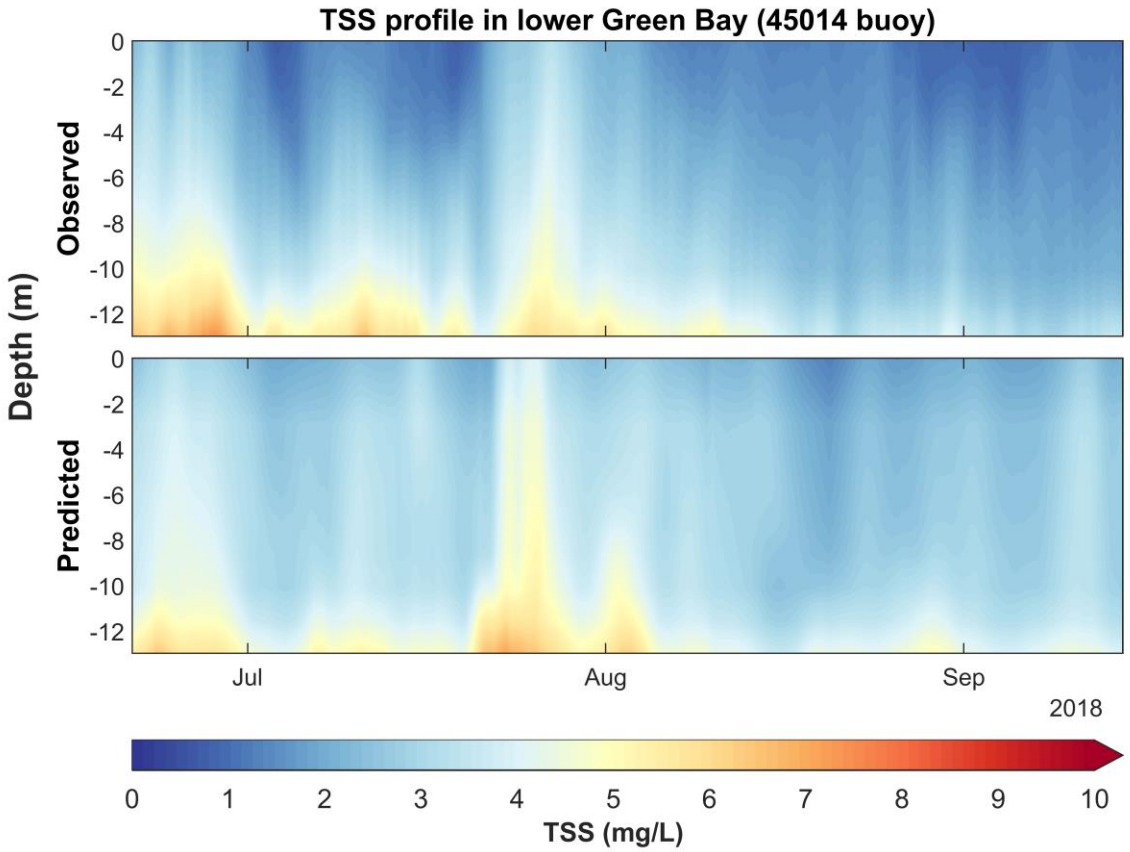

Figure 4. Comparison of the observed and predicted profiles of the total suspended solids (TSS) in lower Green Bay (45014 buoy) in 2018.

5 Results and Discussion: Summer Circulation and Transport Regimes in Lake Michigan and Green Bay

The summer circulation and transport regimes are analyzed in sections 5.1 to 5.4 in terms of monthly average fields of wind-induced currents and waves action, bottom shear stress driven by waves and currents, thermal structure, and sediment transport. The results of this study are shown to complement previous modeling studies of Lake Michigan and to provide important additional details on the circulation and transport regimes in Green Bay. Section 5.5 presents and analyzes a climatological study of the summer circulation and transport regimes in Lake Michigan. Section 5.6 summarizes previous studies on lake sediment dynamics, biogeochemical interactions, HABs, and the role of mussels, and considers the potential application of the approach developed in this study to investigate those processes.

5.1 Monthly-Averaged Wind-induced Circulation and Wave Action

Circulation and wave actions in Lake Michigan are predominantly wind-driven (Beletsky et al., 2006b), and wind affects the exchange between Green Bay and Lake Michigan (Waples & Klump, 2002). Figure 5 shows monthly-averaged wind patterns over Lake Michigan, with higher resolution over Green Bay, during the 2016-2019 simulation period. The figure shows stronger wind fields in northern Lake Michigan, as southerly winds accelerate over the approximately 500 *km* lake's longitudinal fetch. Winds are stronger in July-October with prevailing southwesterly and southerly general regimes. Wind patterns over Green Bay are more uniform, yet consistent with winds over Lake Michigan. Eastern winds dominate in May-June, and the wind fields shift to southwesterly and southerly directions in July until October, when winds are the strongest. Analyses of wind fields in the Great Lakes basin, including Lake Michigan, have shown prevailing southwesterly winds during summer, with monthly and seasonal shifts in wind direction/magnitude during 1980-1999 (Waples & Klump, 2002) and Green Bay during 2004-2008 (Hamidi et al., 2015).

In consistency with previous analyses of monthly averaged circulation in Lake Michigan (Beletsky et al., 2006a), Figure 6 shows that cyclonic (counterclockwise) circulation dominates Lake Michigan. Also, currents drive gyres in the lake, and the formation of gyres is more common in the southern basin. Strong currents at the exchange zone affect water, heat, and sediment fluxes between Lake Michigan and Green Bay. In consistency with wind patterns, circulation is weaker in May and currents accelerate starting in June. Bimonthly analysis of currents in the May-October period in Lake Michigan in 1982-1983 and 1994-1995 also suggests that currents magnitude increase from May to October and currents move counterclockwise and are stronger in the nearshore areas of the southern basin of the lake.

In Green Bay, the currents show more spatial variability than the wind fields, with the widespread formation of gyres, particularly north of Chambers Island and near the exchange zone with Lake Michigan, where strong currents are observed. Currents are generally in the north direction and stronger near the western shore of the bay. Most of these patterns, in particular stronger nearshore currents and frequent formation of gyres in Green Bay during summer, have shown by previous efforts in the simulation of currents in Green Bay for the 2004-2008 period using a POM-based circulation model (Hamidi et al., 2015). Those patterns are present along the

668 water column, although currents are much stronger in the surface (Figures S8 and S9 in the
669 Supporting Information).

670 Current movement and transport in Green Bay are significantly restricted by morphology
671 and lake bottom terrain. Figure 7 shows monthly averaged horizontal current profiles, based on
672 2016-2019 simulations, along the three cross-sections shown in Figure 1. As illustrated in cross-
673 section A-A' (where red colors show northward currents and blue colors show southward
674 currents along the section), the currents in southern Green Bay (i.e., south of Chambers Island,
675 located at *km* 85)—which play a main role in the transport of Fox River loads to the northern
676 bay—shift direction in June and move towards the south in the longitudinal cross-section A-A'.
677 The southward current pattern is driven by a combination of wind direction and cold-water
678 intrusion from the lake into the bay as mentioned above. Current profiles north of Chambers
679 Island and south of the exchange zone (between *km* 85 and *km* 130) are different from the rest of
680 the cross-section. Those patterns can be explained by the presence of gyres in that area,
681 especially away from the shorelines and in the central bay areas where cross-section A-A' cuts
682 through. Figures S8 and S9 in the Supporting information show clearly that the surface currents
683 in Green Bay are predominantly flowing north (especially near the shorelines) and bottom
684 currents flow towards the south, providing more evidence for the summertime stratified flow
685 conditions in the bay.

686 The current patterns in cross-section B-B' (where red colors show northward currents and
687 blue colors show southward currents perpendicular to the section) show that currents in the
688 western side of Chambers Island are strong and predominantly towards the south. The prevailing
689 southward and northward currents through the western and eastern sides of Chambers Island,
690 respectively, imply a counterclockwise circulation around the island, as shown in previous
691 studies based on field observations (Hawley & Niester, 1993). Cross-section B-B' shows that,
692 while surface currents are conveying water north, strong currents are moving towards the south
693 near the bottom. Current profiles at cross-section C-C' (where blue colors show currents flowing
694 into the bay and red colors show currents flowing out perpendicular to the section) also provide
695 evidence that lake cold-water intrusion into the bay occurs persistently through deeper sections
696 of the exchange zone profile. Similar to conditions in Chambers Island, currents are regularly
697 swirling around the small islands in this area.

Currents are the dominant driver of circulation and heat transfer in lake systems, yet waves contribute significantly to sediment dynamics, through bottom interactions and resuspension events. According to Figure 8, wave action in Lake Michigan is limited in May-August, gradually increases in September, and escalates in October. In general, the northern basin of Lake Michigan experiences stronger waves, most probably due to dominant southern winds during the modeling period. The wind-dependency of wave actions in Lake Michigan was shown by previous modeling storm and surge peak events (Mao et al., 2016; Mao & Xia, 2017).

In concert with Lake Michigan, waves in the bay are stronger in September and October. Upper Green Bay and the exchange zone experience stronger waves probably due to rapid change in the bottom elevation in that area. As the incoming waves, originated in deep central areas of Lake Michigan, approach shallow waters of Green Bay and small islands at the connecting straits, water depth quickly starts to become less than the wavelength, reducing wave propagation velocity and leading to steepening of the waves and increased wave height.

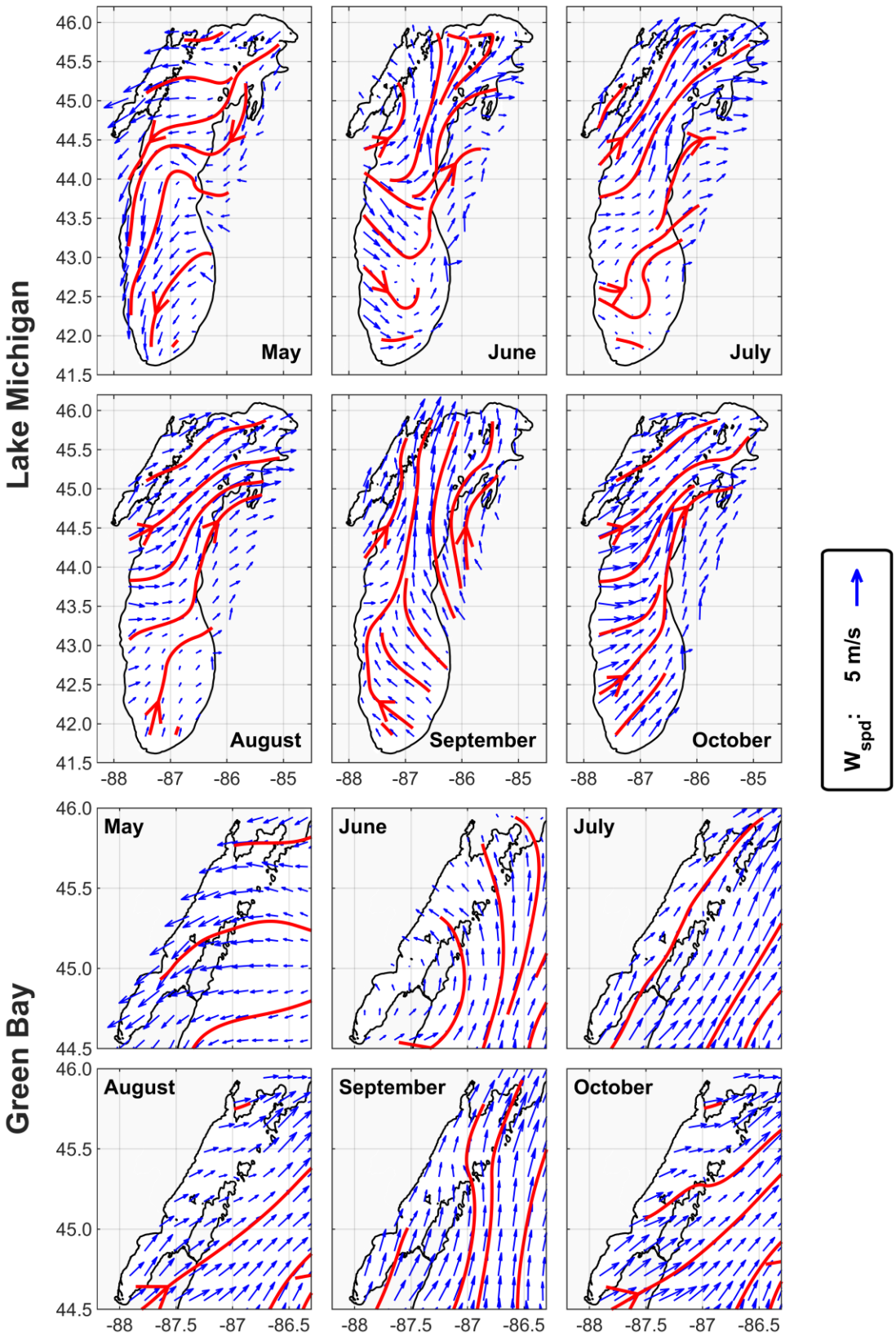

Figure 5. Monthly-averaged wind patterns over the surface of Lake Michigan and Green Bay during the period of 2016-2019 years. Bolded red lines indicate dominant wind patterns. W_{spd} denotes wind speed.

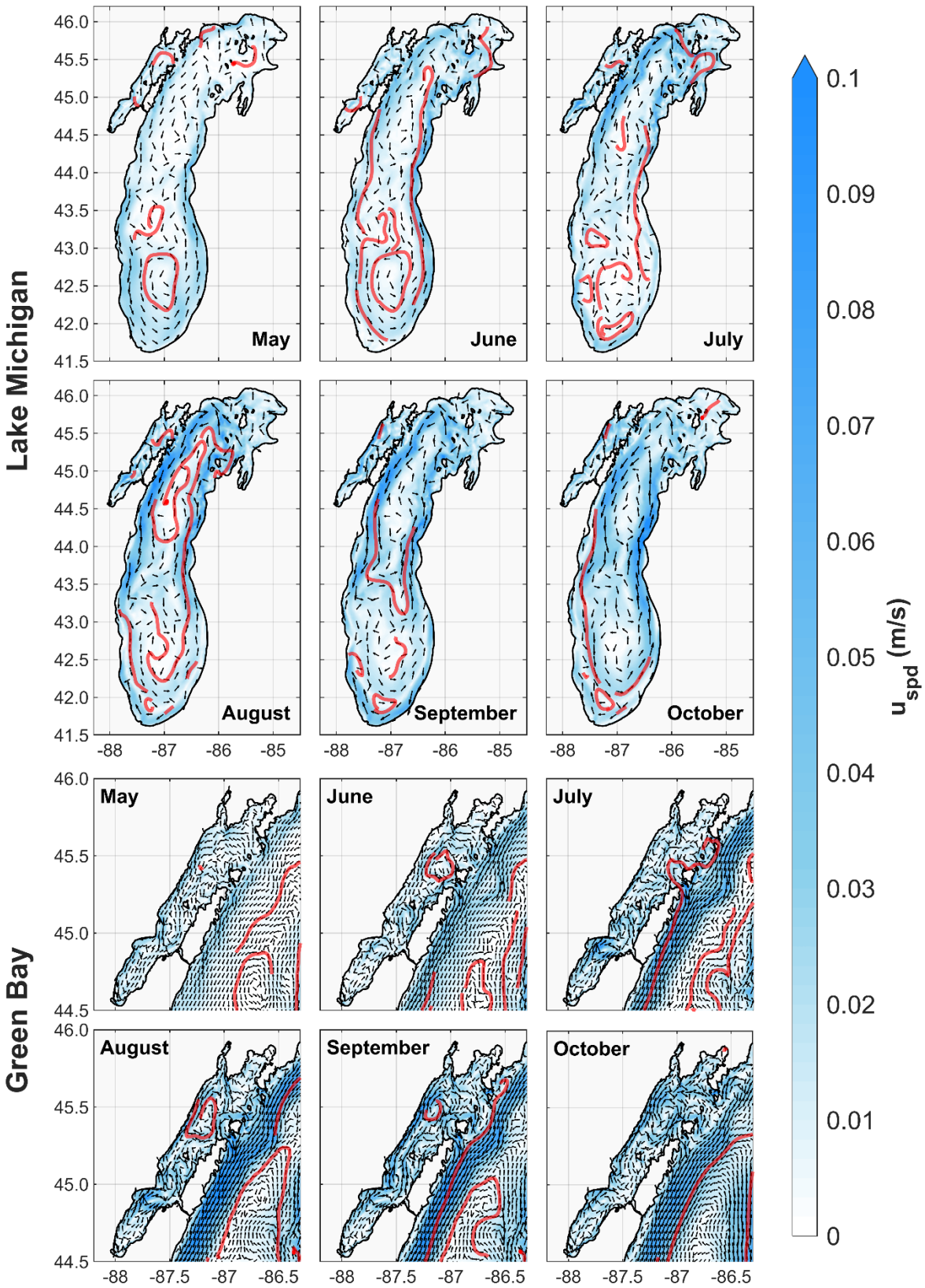

Figure 6. Monthly- and depth-averaged currents in Lake Michigan and Green Bay during the period of 2016-2019 years. Bolded red lines indicate dominant circulation patterns. u_{spd} denotes currents magnitude.

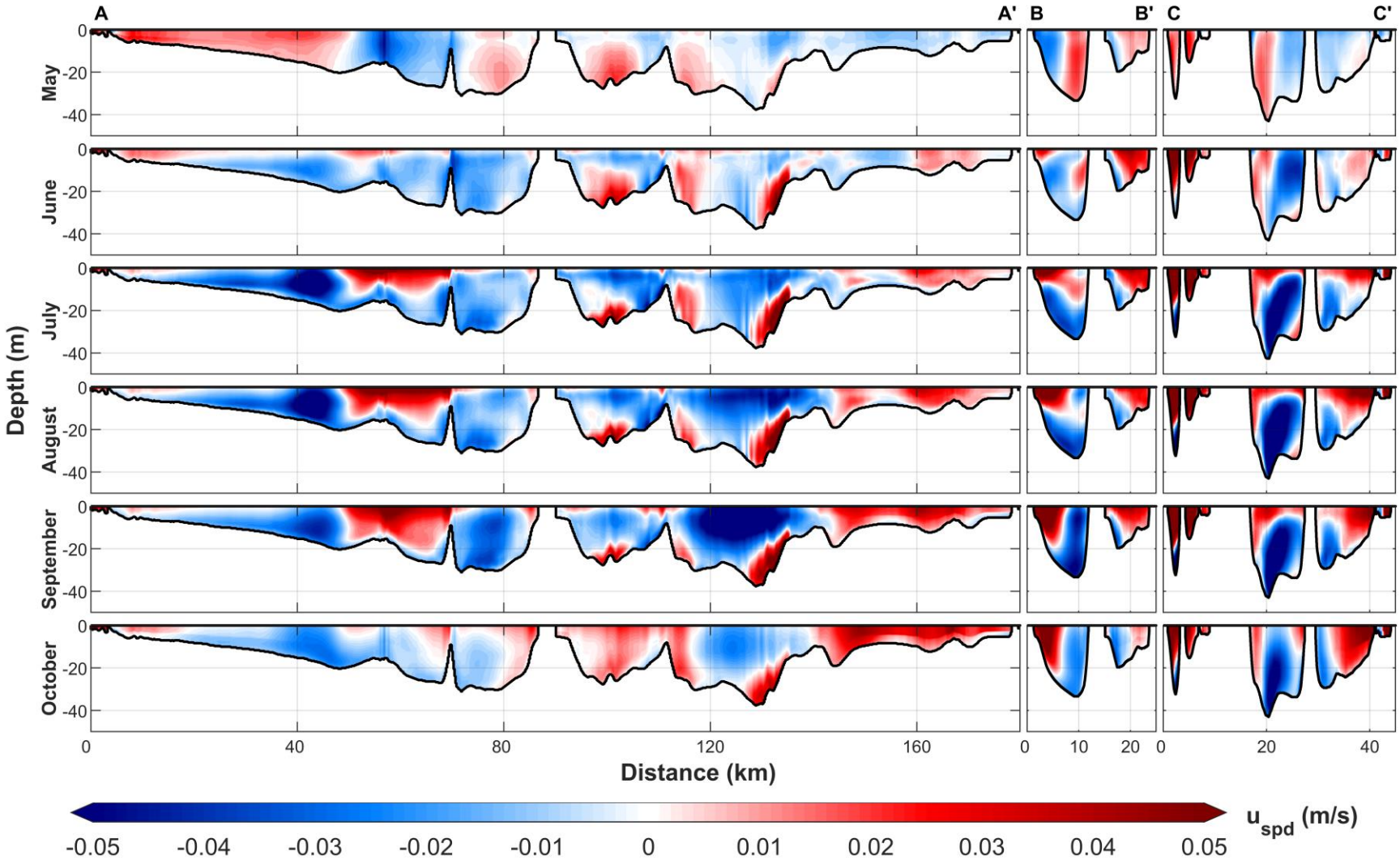

Figure 7. Monthly-averaged current profiles along the A-A' (Green Bay longitudinal axis), B-B' (Chambers Island), and C-C' (connecting straits) cross-sections (as shown in Figure 1) during the period of 2016-2019 years. The vertical axis is exaggerated ~700 times. u_{spd} denotes currents magnitude. Colors show current directions along the A-A' cross-section (red/blue indicates northward/southward) and perpendicular to B-B' and C-C' cross-sections (red/blue indicates into/out of cross-sections, respectively).

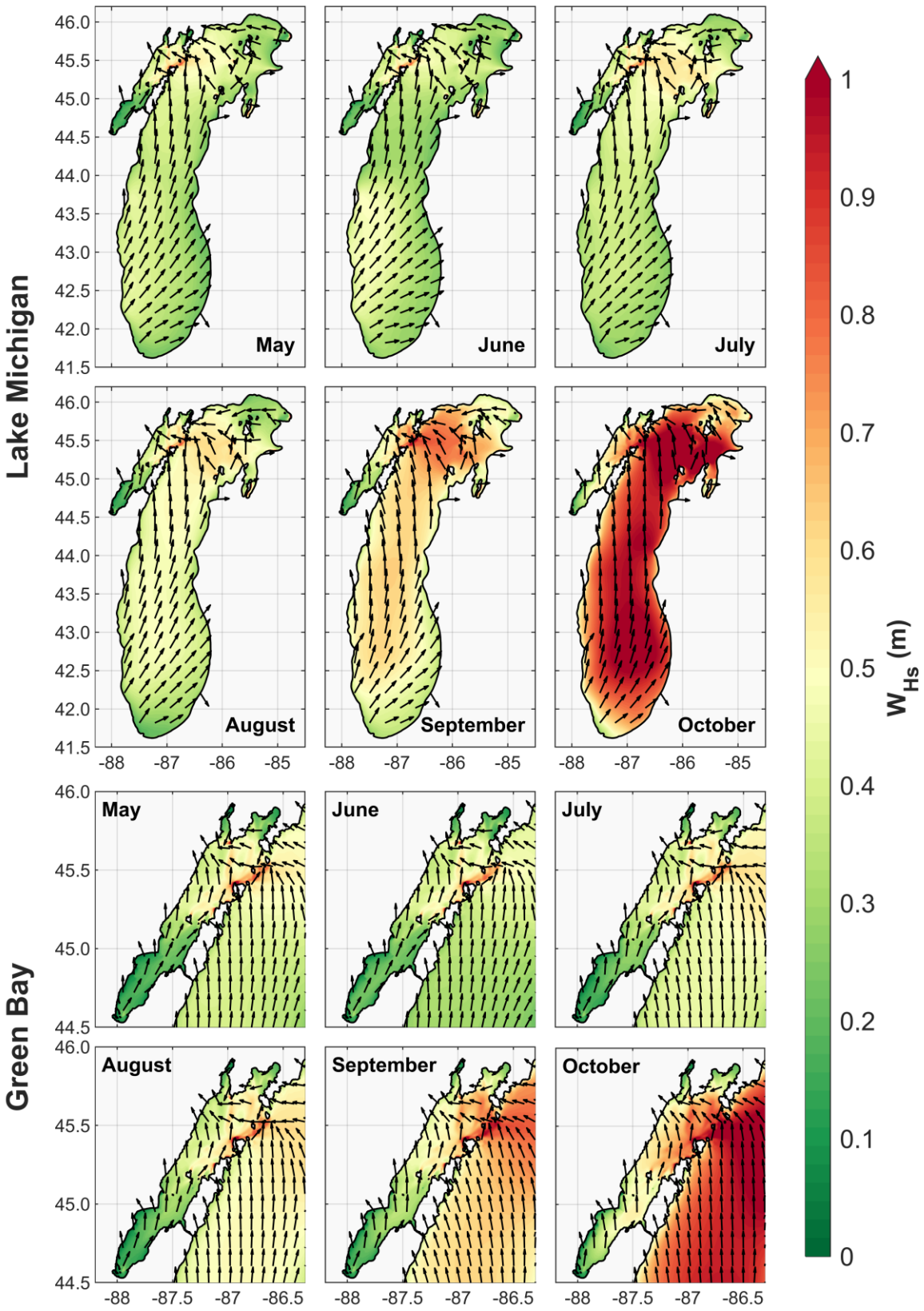

Figure 8. Monthly-averaged significant wave height (W_{Hs}) in Lake Michigan and Green Bay during the period of 2016-2019 years.

5.2 Current-Wave Induced Bottom Shear Stress

Bottom shear stress governs resuspension events and sediment availability in the water column. Figure 9 shows the calculated monthly-averaged bottom shear stress due to the combined effects of current-wave action. While higher shear stress near coastal areas is associated with the stronger nearshore currents, increased wave action in September and October results in augmented shear stress during those months. Western coastal regions, southern and northern shallow areas, and the connecting straits experience higher stress in Green Bay. Also, one would expect strong and frequent resuspension to occur in lower Green Bay in October, produced by the bottom shear stress forcing patterns during that month. Increased shear stress in southwestern Lake Michigan during May is probably associated with a lake-wide cyclonic gyre in the southern basin driven by widespread and strong northerly winds in that area. Southwestern coastal areas of Lake Michigan do not experience such strong wind regimes again until October. Those patterns, in particular high shear stress in the southern and western nearshore areas of Lake Michigan and southern, western, and northern Green Bay, compare well with current and wave bed shear distribution during a March 1998 episode shown by Lee et al. (2007), as well as average shear stress patterns in Lake Michigan during 1994-1995 (Lou et al., 2000).

To investigate the distinct contribution of waves and currents in driving physical forces in the lake, we simulated bottom shear stress without waves (currents only) and compared the results with the combined current-wave conditions. As expected, results indicated that for the May-October period of 2016-2019 years, on average the bottom shear stresses were higher by 494%, 334%, and 296% in Lake Michigan, Green Bay, and lower Green Bay, respectively, when combined physical processes are considered, compared to the case when only currents are driving bottom shear stresses. Figure S10 and Table S1 in the Supporting Information compare the average spatial patterns of bottom shear stress in Lake Michigan and Green Bay under the two different physical forcing scenarios for the simulation period of 2016-2019 years. We expect to observe similar impact on *TSS* patterns in the lake due to these different driving stress scenarios. It is obvious that current-wave-induced forces play an important role in sediment plume development and transport. As shown in previous studies, the effects of waves are significant in shallow nearshore waters of Lake Michigan and Green Bay (Lou et al., 2000).

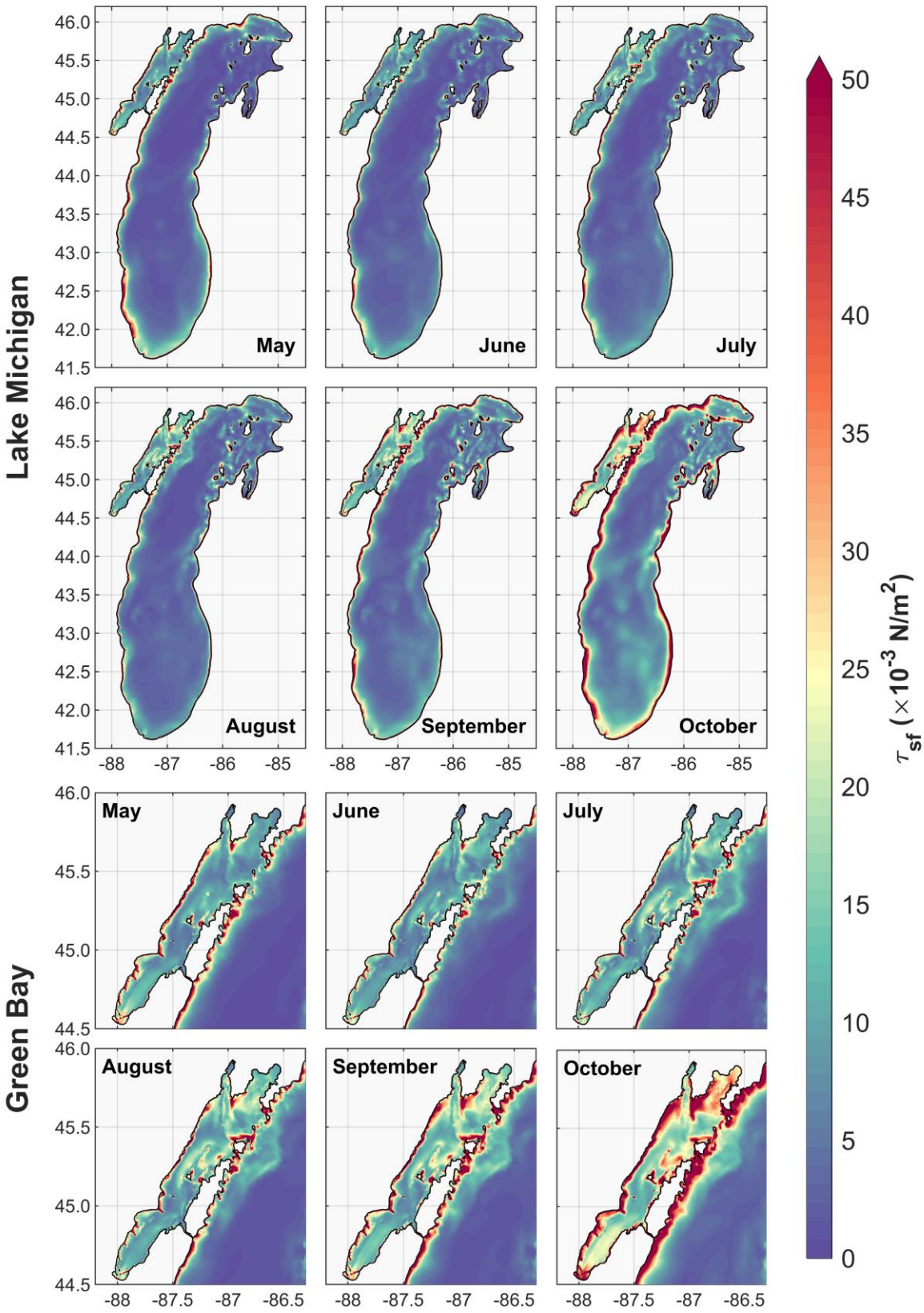

Figure 9. Monthly-averaged bottom shear stress (τ_{sf}) due to combined effects of currents and waves in Lake Michigan and Green Bay during the period of 2016-2019 years.

5.3 Thermal Structure of the system

Lake Michigan May-October monthly averages surface temperature fields are illustrated in Figure 10, based on 2016-2019 simulations. The southern basin of Lake Michigan is generally warmer than the rest of the lake. Driven by dominant wind direction and coastal upwellings, western nearshore areas of the lake are often slightly colder than the open lake and eastern coastlines. These patterns were also observed by POM-based simulations of thermal structure in Lake Michigan during May-October of 1982-1983 and 1994-1995 (Beletsky & Schwab, 2001). The thermal regime in Green Bay is significantly different than that of Lake Michigan. Warmer temperatures in the bay can be explained by weaker mixing and shallower morphology. July-September are the months with more spatial variability, with higher temperatures in the southern and northern shallow areas, and colder waters near the exchange zone with Lake Michigan, predominantly due to cold water intrusions from the lake.

Stratification is an important aspect of the thermal regime and circulation, and consequently of the ecological functioning of the bay. Figure 11 shows monthly average temperature profiles, based on 2016-2019 simulations, along the three cross-sections shown in Figure 1. The results of this study are consistent with the findings by Hamidi et al. (2015, 2013) and Bravo et al. (2015), showing that stratification in Green Bay starts in June, peaks in July and August, and starts to fade in September, resulting in a duration of about three months. Cross-section A-A' shows that vertical mixing of temperature occurs at faster rates in shallower areas, as expected. The Fox River has a significant influence on the thermal distribution of the southern Green Bay as shown in the first 50 *km* of the cross-section A-A' temperature profiles, closer to the mouth of the Fox River. Cross-section B-B' shows that the temperature gradient is stronger in the western side channel of Chambers Island section compared to the well-mixed, shallower eastern channel. Stratification patterns are preserved at cross-section C-C', where Green Bay meets Lake Michigan, but with a weaker gradient.

One advantage of FVCOM is its ability to capture upwelling events in coastal areas of Lake Michigan. A comparison of simultaneous wind fields, surface currents, and surface temperature fields indicates that northerly and southerly winds promote upwellings on the western and eastern coastal areas, respectively (Figure S12 in the Supporting Information). This

787 is an important quality when physical models are used to study biogeochemical processes in lake
788 systems.

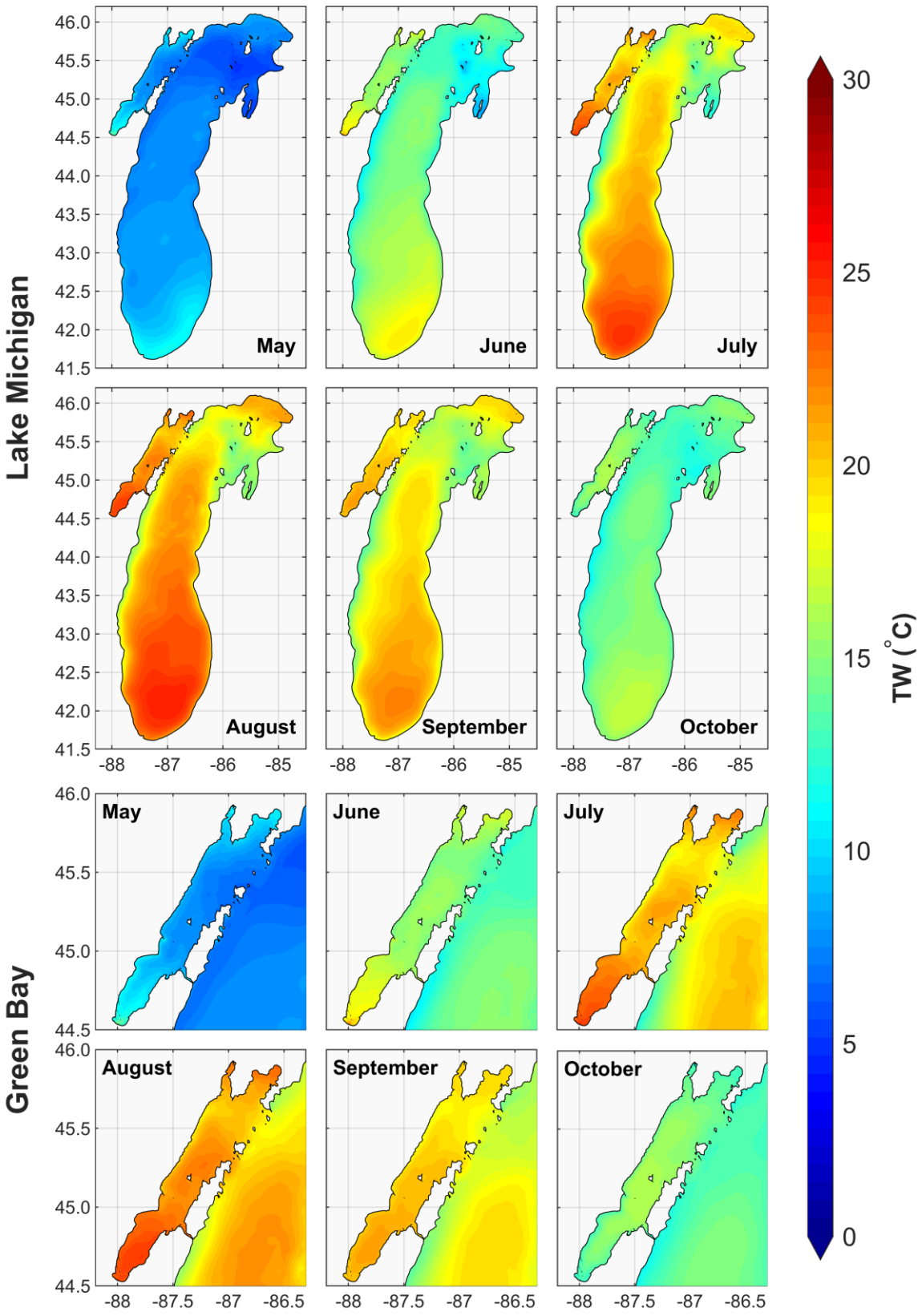

Figure 10. Monthly-averaged surface temperature fields (TW) in Lake Michigan and Green Bay during the period of 2016-2019 years.

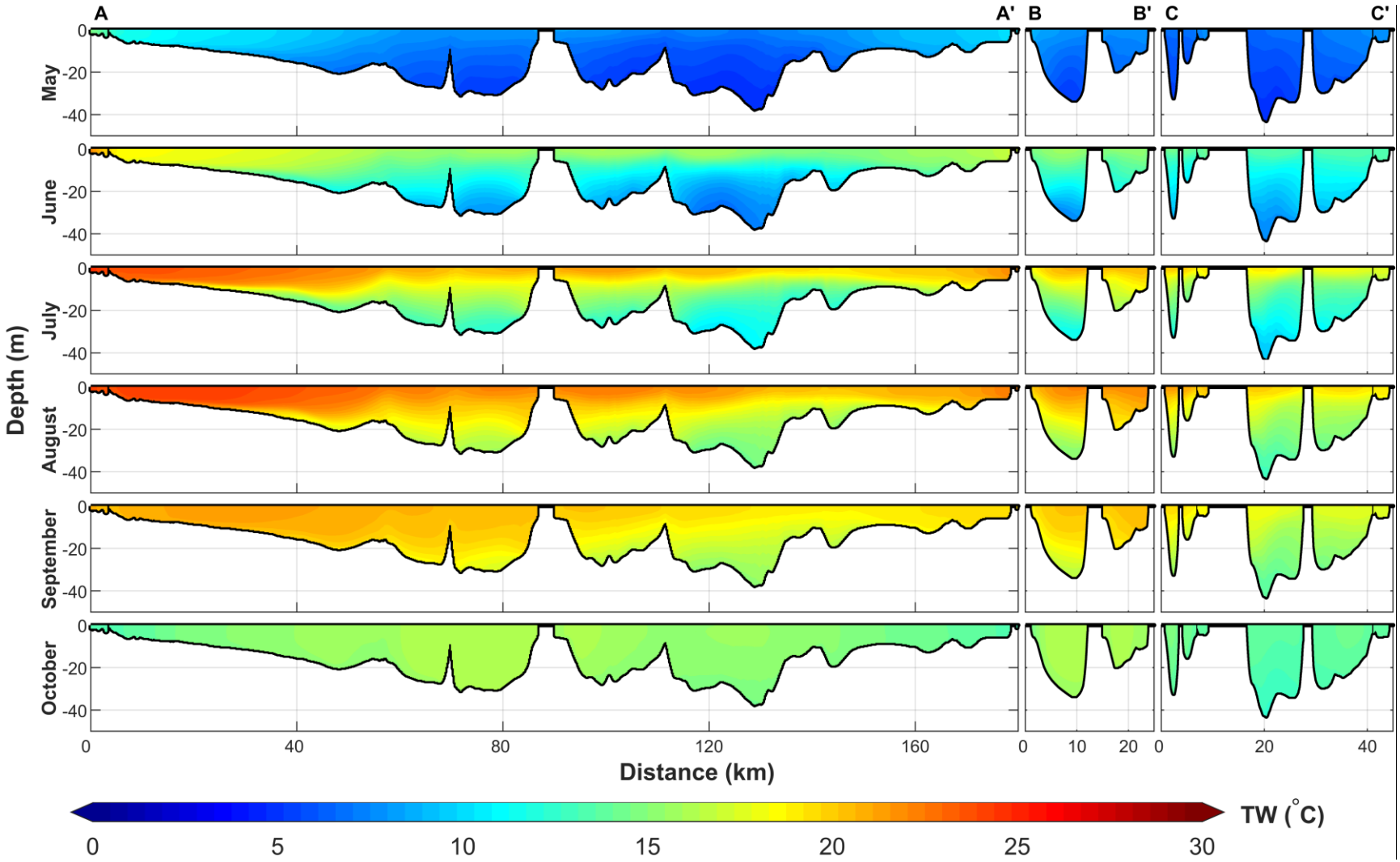

Figure 11. Monthly-averaged water temperature (TW) profiles along the A-A' (Green Bay longitudinal axis), B-B' (Chambers Island), and C-C' (connecting straits) cross-sections (as shown in Figure 1) during the period of 2016-2019 years. The vertical axis is exaggerated ~700 times.

5.4 Sediment Transport

Figure 12 shows May-October monthly- and depth-averaged simulated *TSS* concentration in Lake Michigan, with higher resolution in Green Bay, based on 2016-2019 simulations. Consistent with shear stress patterns shown in Figure 9, *TSS* concentration patterns are relatively uniform June through September, with higher concentrations in May and October in the southernmost and northernmost Lake Michigan nearshore areas, as well as southern Green Bay. Periods of resuspension in southwestern Lake Michigan during May are related to wind-driven strong bottom shear stress and the availability of fine-grained sediments in those areas. In almost every month southern Green Bay and southern Lake Michigan experience higher *TSS* concentrations than the rest of the lake. These patterns are similar to those presented by Lee et al. (2007) for March 1998 episodic events, based on physical simulations of sediment transport and satellite imagery-based maps of sediment concentration (Figures 8 and 9 in that article). Also, those patterns qualitatively resemble the predicted TSS concentration in southern Lake Michigan during the 1994-1995 period (Lou et al., 2000).

Sediment transport in Green Bay shows significant differences with the transport patterns in Lake Michigan. The Fox River acts as a point source of *TSS*, and the southern bay shows high *TSS* concentrations every month, while the northern bay is more influenced by the Lake Michigan patterns of transport. In Upper Green Bay the sediment transport is consistent with shear stress patterns and mostly influenced by circulation and waves. The *TSS* spatial distribution in the southern bay seems to be governed by the Fox River persistent and significant *TSS* loading, and by the abundance of fine-grained sediments.

An interesting observation in the patterns of sediment circulation in Green Bay is that *TSS* concentration is frequently higher in eastern nearshore areas of lower Green Bay, despite higher current-wave driven shear stresses in the western shorelines. One possible explanation is that the river plume tends to flow along the eastern shore because of the frequent counterclockwise circulation in the southern bay driven by wind direction and the Coriolis effect. In addition, several islands in western Green Bay (shown in Figure S2 in the Supporting Information) cause less and/or weaker resuspensions in that area, therefore, the eastern shore contains more sediments, produced mainly by resuspension, than waters near the western shore. That model result is consistent with Klump et al.'s (1997) finding that currents carrying the

plume of turbid Fox River water north along the eastern shore of the bay turn westward off Sturgeon Bay in a counterclockwise gyre that leaves behind a blanket of fine slit accumulating at rates of up to ~1 *cm/year* (160 *mg/cm^2/year*), 20 times faster than the average for the southern bay as a whole.

The *TSS* concentration profiles along the A-A' longitudinal cross-section of Green Bay, shown in Figure 13, show more sediment dynamics near the mouth of Fox River (point A) and higher *TSS* concentrations in the shallow southern and northern ends of the bay at points A and A'. The model results show less variability in *TSS* concentration at the Chambers Island (B-B') and connecting straits (C-C') cross-sections. Higher sediment concentration west of Chambers Island cross-section (point B) is probably due to stronger currents near the western shoreline. Results also showed higher sediment transport through channels on the north side of the connecting straits (near point C'), probably due to higher shear stresses in that area.

As we discussed in Section 5.4, combined current-wave actions drive stronger shear stresses at the water-sediment interface, implying more intense resuspension and transport near the bottom. Our analysis showed that on average during the May-October period of 2016-2019 years, considering current-wave combined effects results in 43%, 39%, and 32% higher depth-averaged TSS concentration, respectively, in Lake Michigan, Green Bay, and lower Green Bay in comparison with the case when currents are the sole driver of physical forcing in the lake. *TSS* patterns in Lake Michigan and Green Bay are illustrated with more details in Figure S11 and Table S2 in the Supporting Information.

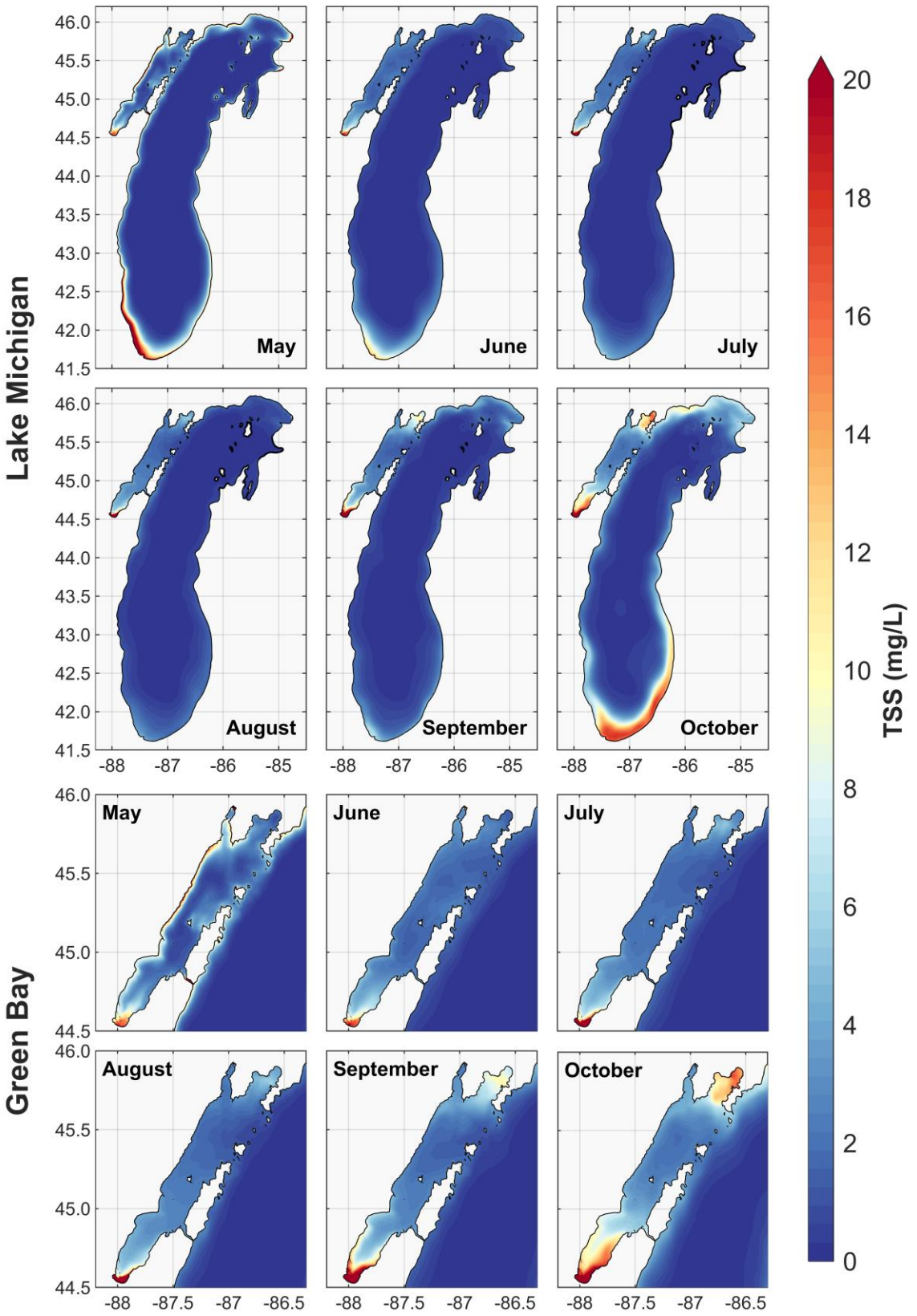

Figure 12. Monthly- and depth-averaged total suspended solids (TSS) in Lake Michigan and Green Bay during the period of 2016-2019 years.

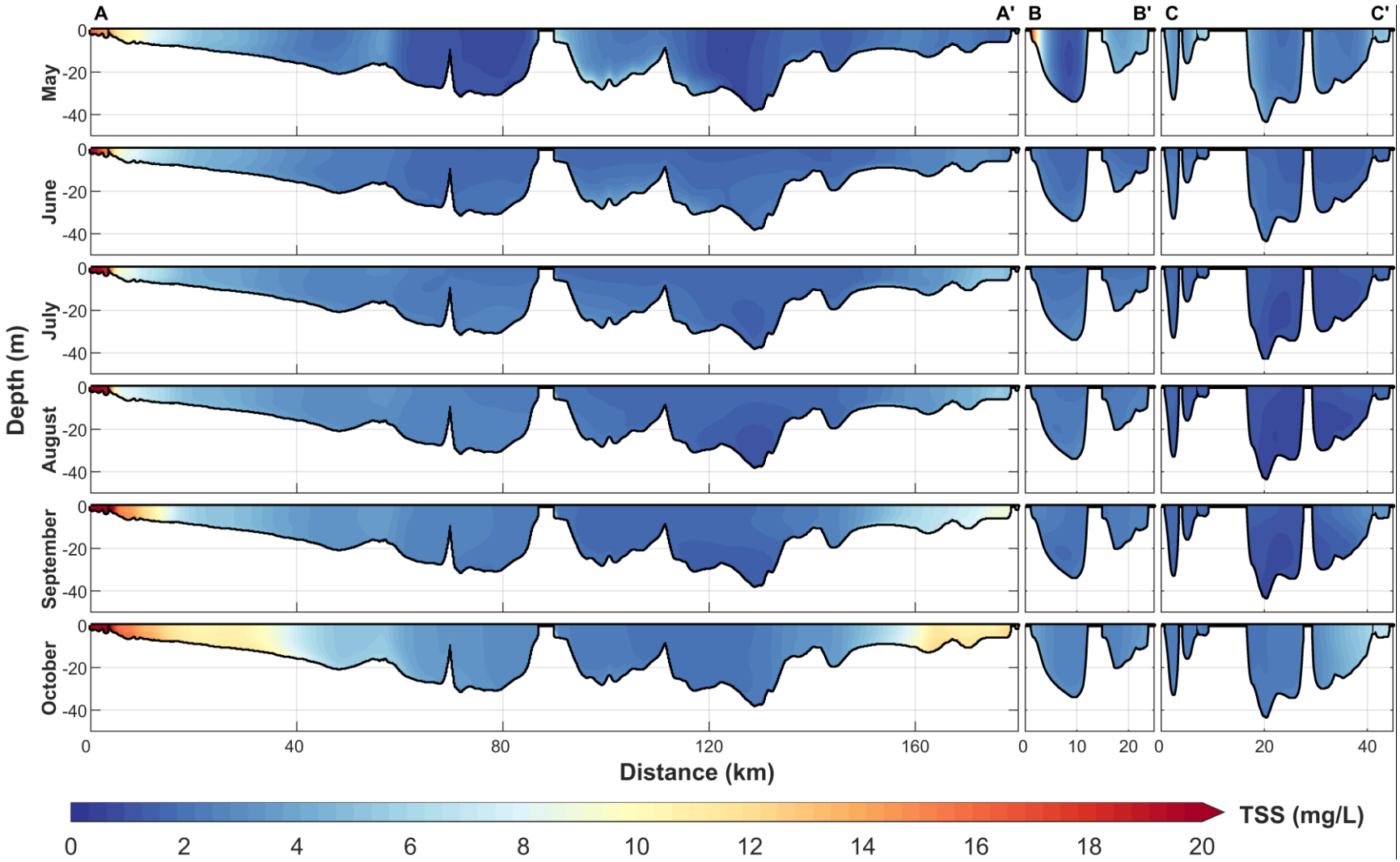

Figure 13. Monthly-averaged total suspended solids (TSS) profiles along the A-A' (Green Bay longitudinal axis), B-B' (Chambers Island), and C-C' (connecting straits) cross-sections (as shown in Figure 1) during the period of 2016-2019 years. The vertical axis is exaggerated ~700 times.

5.5 Climatological Summer Circulation and Sediment Transport Patterns in Lake Michigan

This section aims to provide maps of summer transport of heat and sediment in Lake Michigan, based simulations using the 2016-2019 meteorological forcing. Figure 14 shows that in general, the prevailing wind direction is southwesterly, and winds are stronger in northern Lake Michigan. The spatial distribution of bottom shear stress shows consistency from year to year, with stronger stresses occurring in southwestern Lake Michigan, Green Bay, and nearshore areas. The maps of surface temperature show a negative, gradual gradient from south to north and a small decline in surface temperature in the southern basin of the lake from 2016 to 2019. The climatological summer surface water temperature in Green Bay was fairly uniform during the simulation period, except that it was somewhat colder near the exchange zone with Lake Michigan.

The map of *TSS* concentration was fairly steady during the simulation period, but there was a small decrease in *TSS* concentration in southwestern Lake Michigan from 2016 to 2019. That temporal pattern was consistent with decreasing winds over the southern lake surface during that period. Northern Lake Michigan showed neither temporal variability in *TSS* patterns nor dependency on wind fields. Those results imply that sediment dynamics in the southern basin is more sensitive to wind and meteorological variability. That is an important pattern to be considered in coastal conservation and shoreline protection.

The maps of *TSS* concentration showed a different temporal trend in lower Green Bay compared to the whole lake. While *TSS* concentration showed a decreasing temporal trend in southern Lake Michigan, sediment concentration increased in lower Green Bay between 2016 and 2019. The increase is probably due to increased loading rates into the bay and confirms the importance of including the tributary loads, especially from the Fox River in modeling sediment transport and biogeochemical interactions in Green Bay.

The findings of this research confirm the results of previous studies by showing the importance of wind forcing in the circulation and transport in Lake Michigan. Wind forcing is a primary driver of circulation in Lake Michigan and Green Bay and can influence biogeochemical processes by governing the thermal structure of the lake and the fate and transport of sediments. Wind patterns should be given particular attention in restoration studies for Green Bay.

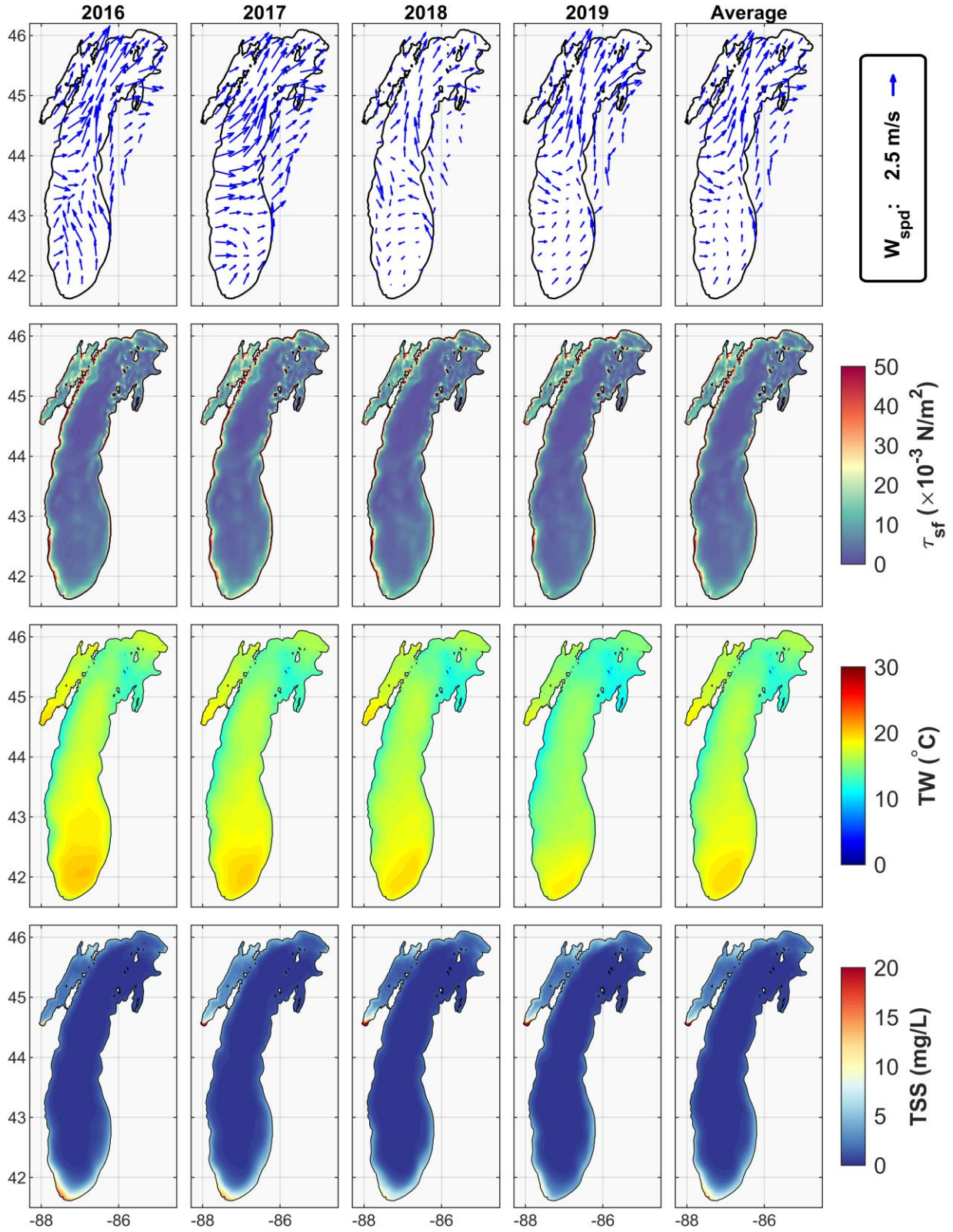

Figure 14. Average annual wind fields (W_{spd}), current-wave driven bottom shear stress (τ_{sf}), surface temperature fields (TW), and depth-averaged total suspended solids (TSS) in Lake Michigan during the period of 2016-2019 years. The last column shows the average for four simulated years.

5.6 Context and scope of this research

The 2017 "Summit on the Ecological and Socio-Economic Tradeoffs of Restoration in the Green Bay, Lake Michigan Ecosystem" (Klump et al., 2018) looked at the state of knowledge, gaps, and monitoring needs in the key areas of watershed modeling, biogeochemistry and hydrodynamics, ecosystem modeling and trophic dynamics, habitat and diversity, and socioeconomic and management issues. The introduction of this article summarized the gaps identified in biogeochemistry and hydrodynamics and the intended contribution of this research. This section summarizes previous studies on lake sediment dynamics, biogeochemical interactions, HABs, and the role of mussels, and considers the potential expansion of this model to study those processes. Bartlett et al.'s (2018) is the first study of its kind to assess the spatial diversity of cyanotoxins in Green Bay, Lake Michigan. They characterized the diversity and spatial distribution of toxic or otherwise bioactive cyanobacterial peptides (TBPs) in Green Bay. They collected samples during three cruises in August 2014, and July and August 2015 at sites spanning the mouth of the Fox River north to Chambers Island. They found that microcystins (MCs) were positively correlated with chlorophyll (Chl) and negatively correlated with distance to the Fox River in all cruises along a well-established south-to-north trophic gradient in Green Bay. The influx of nutrients combined with shallow waters in the lower bay creates an ideal environment for the proliferation of cyanobacteria and the formation of Cyanobacterial harmful algal blooms (cyanoHABs).

Luo et al. (2012) simulated a 1998 spring phytoplankton bloom in Lake Michigan using a coupled physical-biological model. Their biological model was a nutrient-phytoplankton-zooplankton-detritus (NPZD) model, that included phosphorus as the nutrient, phytoplankton, zooplankton, and detritus. The biological model was coupled with the FVCOM physical model and included a wind-wave mixing parametrization but no sediment transport. They searched for the main physical and ecological mechanisms of this spring bloom formation and decay over a long-time scale during March to May, differing from the previous studies of the short-term (5-7 days in March) bloom processes. They confirmed that the phytoplankton bloom was forced by rapidly increasing temperature and light intensity in spring. The thermal front that developed in spring inhibited the transport of nutrients and phytoplankton from the nearshore to the deeper water. The wind-driven gyre circulation in southern Lake Michigan induced significant offshore transport, which contributed to the establishment of the circular bloom. To test the importance of

general circulation and interior source of ecological factors in the lake for sustaining the donut-like spring bloom, the phosphorus released from suspended sediments and rivers were excluded from their study.

Shen (2016) applied a 1D biophysical model and FVCOM to investigate the ecosystem of Lake Michigan, specifically to explore how invasive mussels affect the nutrient dynamics and distribution of phytoplankton. Wave effects were considered in the 1D biophysical model, but not in the 3D FVCOM simulations. Rowe et al. (2017) used a biophysical model to study the influence of invasive quagga mussels, phosphorus loads, and climate on spatial and temporal patterns of productivity in Lake Michigan. They applied the FVCOM hydrodynamic model, and the FVCOM general ecosystem module (GEM) to implement the NPZD model with the addition of a fifth compartment to represent benthic filter feeder (dreissenid mussel) biomass. They found that although Chl-a and primary production declined over the quagga mussel invasion, their results suggested that increased nutrient loads would increase lake-wide productivity even in the presence of mussels; however, altered spatial and temporal patterns of productivity caused by mussel filter feeding would likely persist. Rowe et al.'s (2017) model included neither a wave model nor a sediment transport model.

Bravo et al. (2019) linked a previously built hydrodynamic model and a water quality model developed by Fillingham (2015), extended to three dimensions to simulate the transport and fate of phosphorus in the nearshore area of Lake Michigan. Their model accounted for the interactions between phosphorus, Cladophora, mussels, and lake sediments in the nearshore zone. They quantified the lake assimilative capacity by applying their model to estimate the area required for mixing and diluting wastewater treatment plant outfall total phosphorus loadings to the level of the lake target concentration during the Cladophora growing season. Their model results compared well with empirical measurements of particulate and dissolved phosphorus as well as Cladophora biomass and phosphorus content. The model was applied to test scenarios of wastewater treatment plant phosphorus loading in two different years, in order to help establish phosphorus discharge limits for the plant.

The stage is set to apply the approach developed in this study, which includes wave and sediment transport simulation, as follows: a) to study the spatial and temporal variability of cyanotoxins in Green Bay building upon Bartlett et al.’s (2018) spatial analysis; b) to study algal

blooms in lakes following Luo et al.'s (2012) coupled physical-biological modeling approach; c) to improve the study of the influence of invasive quagga mussels on lakes ecosystems pursuing Rowe et al.'s (2017) modeling methods; and d) to study the interactions between phosphorus, Cladophora, mussels, and lake sediments by using the biophysical concepts developed by Bravo et al. (2019).

Ongoing research will apply the model to: a) to evaluate sediment dynamics in the bay under different climate conditions and loading scenarios in river/watershed management; b) predicting the short- and long-term effects of the Cat Island Chain restoration in altering flow, transport, deposition and benthic habitat in the Area of Concern (AOC); and c) to establish a sediment budget for lower- and entire Green Bay. One of the principal goals of the Cat Island Chain restoration project was to reestablish a barrier island complex and reduce wave energy in the inner bay as a means of reducing resuspension and increasing water clarity.

6 Conclusions

The hydrodynamic, wind-wave, and sediment transport model developed in this study includes in a single platform of all the relevant geophysical drivers, namely the momentum flux generated by wind, the heat flux across the water surface, the Earth's rotation, thermal stratification, and topography. The single model of Lake Michigan and its Green Bay estuary has high resolution in the bay and in the exchange zone between the open lake and the bay. The single-model approach provides the desired resolution in the bay estuary and represents the combined effects of tributary flows and lake intrusions. The model overcomes limitations of previous nested models of the estuary that used potentially problematic open boundary conditions to represent the exchange of mass, energy, and momentum with Lake Michigan, and of previous whole-lake models that lacked the desired high resolution in the bay or did not include physically-based wind-wave and sediment transport modules. The model confirms the findings of previous studies on Lake Michigan and demonstrates how the circulation, thermal regime, wind action, and sediment transport in the Green Bay estuary depend on meteorological forcing, tributary flows, and lake water intrusions.

Winds are a primary driver of circulation and wave action in Lake Michigan. Eastern winds dominate in May-June, and the wind fields shift to southwesterly and southerly directions

in July until October, when winds are the strongest. Cyclonic (counterclockwise) circulation dominates Lake Michigan, and the formation of gyres is more common in the southern basin. In consistency with wind patterns, circulation is weaker in May and currents accelerate starting in June. Wave action in Lake Michigan is limited in May-August, gradually increases in September, and escalates in October. The northern basin of Lake Michigan experiences stronger waves due to dominant southern winds. Winds drive the fluxes of water, heat, and sediment between the lake and the estuary. In Green Bay, the currents show more spatial variability than the wind fields, with widespread formation of gyres. Surface currents in Green Bay flow predominantly north (especially near the shorelines) and bottom currents flow predominantly towards the south, providing evidence that the interaction of tributary flows and lake currents force summertime stratified flow conditions in the bay. In concert with Lake Michigan, waves in the bay are stronger in September and October. Upper Green Bay and the exchange zone experience stronger waves due to rapid change in the bottom elevation in that area.

The southern basin of Lake Michigan is generally warmer than the rest of the lake. Driven by dominant wind direction and coastal upwellings, western nearshore areas of the lake are often slightly colder than the open lake and eastern coastlines. Analysis of simultaneous wind fields, surface currents, and surface temperature fields indicates that northerly and southerly winds promote upwellings on the western and eastern coastal areas, respectively. The model's ability to capture upwelling events is an important quality in the study of biogeochemical processes in lake systems. Warmer temperatures in the bay are explained by weaker mixing and shallower morphology. Stratification in Green Bay starts in June, peaks in July and August, and starts to fade in September, resulting in a duration of about three months. Field data and model results showed that the Fox River has a significant influence on the thermal distribution of southern Green Bay.

Total suspended sediment (*TSS*) concentration fields in Lake Michigan are relatively uniform June through September, concentrations are higher in May and October in the southernmost and northernmost Lake Michigan nearshore areas, and in southern Green Bay. Sediment transport in the estuary is clearly shaped by both tributary loads and exchanges with Lake Michigan. The southern bay shows high *TSS* concentrations because the Fox River acts as a main point source of sediments. The Fox River plume tends to flow along the eastern shore because of counterclockwise circulation in the southern bay driven by wind direction and the

Coriolis effect, and consequently, *TSS* concentration is normally higher in the eastern nearshore areas of lower Green Bay. Upper Green Bay is more influenced by current and wave exchanges with Lake Michigan. Sediment transport is higher through the channels on the north side of the connecting straits, because of higher shear stresses in that area.

Acknowledgments

This project was funded partially by the University of Wisconsin Sea Grant Omnibus Program Grant 144-AAG3496-UWMKE19A. We appreciate Jeff Houghton for assistance in the fieldwork, Jim Wagner and Jason Bacon for IT support, and Jessie Grow, Dr. Sarah Bartlett, and Dr. Todd Miller for providing field data in Green Bay and Lake Michigan.

Lake Michigan bathymetry and shoreline data are obtained from NOAA National Geophysical Data Center (http://maps.ngdc.noaa.gov/viewers/bathymetry/). Input meteorological forcing data is based on NOAA National Centers for Environmental Information (https://www.ncei.noaa.gov/). Buoy observations were also downloaded from NOAA National Data Buoy Center (https://www.ndbc.noaa.gov/), Great Lakes Observing System (https://uwm.edu/glos/), *lakestat* monitoring program (http://www.lakestat.com/), and USGS National Water Information System (NWIS) database (https://waterdata.usgs.gov/nwis). River inputs are also based on the USGS NWIS database. Lake Michigan water level data is downloaded from NOAA Tides and Currents dataset (https://tidesandcurrents.noaa.gov/stations.html?type=Water+Levels). Turbidity and *TSS* in-situ observations at the mouth of Fox River are provided based on personal communications with Dr. Sarah Bartlett at the NEW Water (http://newwater.us/programs-initiatives/aquatic-monitoring-program/). MODIS imagery products are obtained from the NASA EARTHDATA platform (https://earthdata.nasa.gov/). This is GLERL contribution number XXXX.

References

Anderson, E. J., & Phanikumar, M. S. (2011). Surface storage dynamics in large rivers: Comparing three-dimensional particle transport, one-dimensional fractional derivative, and multirate transient storage models. *Water Resources Research, 47*(9). https://doi.org/10.1029/2010WR010228

Anderson, E. J., & Schwab, D. J. (2011). Relationships between wind-driven and hydraulic flow

in Lake St. Clair and the St. Clair River Delta. *Journal of Great Lakes Research*, *37*(1), 147–158. https://doi.org/10.1016/J.JGLR.2010.11.007

Anderson, E. J., & Schwab, D. J. (2013). Predicting the oscillating bi-directional exchange flow in the Straits of Mackinac. *Journal of Great Lakes Research*, *39*(4), 663–671. https://doi.org/10.1016/j.jglr.2013.09.001

Anderson, E. J., Schwab, D. J., & Lang, G. A. (2010). Real-Time Hydraulic and Hydrodynamic Model of the St. Clair River, Lake St. Clair, Detroit River System. *Journal of Hydraulic Engineering*, *136*(8), 507–518. https://doi.org/10.1061/(ASCE)HY.1943-7900.0000203

Anderson, E. J., Stow, C. A., Gronewold, A. D., Mason, L. A., McCormick, M. J., Qian, S. S., et al. (2021). Seasonal overturn and stratification changes drive deep-water warming in one of Earth's largest lakes. *Nature Communications*, *12*(1), 1688. https://doi.org/10.1038/s41467-021-21971-1

Ariathurai, R., & Arulanandan, K. (1978). Erosion Rates of Cohesive Soils. *J Hydr Div, ASCE*, *101*(5), 635–639.

Bai, X., Wang, J., Schwab, D. J., Yang, Y., Luo, L., Leshkevich, G. A., & Liu, S. (2013). Modeling 1993–2008 climatology of seasonal general circulation and thermal structure in the Great Lakes using FVCOM. *Ocean Modelling*, *65*, 40–63. https://doi.org/10.1016/J.OCEMOD.2013.02.003

Battjes, J. A., & Janssen, J. P. F. M. (1978). Energy Loss and Set-Up Due to Breaking of Random Waves. In *Coastal Engineering 1978* (pp. 569–587). New York, NY: American Society of Civil Engineers. https://doi.org/10.1061/9780872621909.034

Beletsky, D., & Schwab, D. J. (2001). Modeling circulation and thermal structure in Lake Michigan: Annual cycle and interannual variability. *Journal of Geophysical Research: Oceans*, *106*(C9), 19745–19771. https://doi.org/10.1029/2000JC000691

Beletsky, D., O'Connor, W. P., Schwab, D. J., Dietrich, D. E., Beletsky, D., O'Connor, W. P., et al. (1997). Numerical Simulation of Internal Kelvin Waves and Coastal Upwelling Fronts*. *Http://Dx.Doi.Org/10.1175/1520-0485(1997)027<1197:NSOIKW>2.0.CO;2*. https://doi.org/10.1175/1520-0485(1997)027<1197:NSOIKW>2.0.CO;2

Beletsky, D., Schwab, D. J., Roebber, P. J., McCormick, M. J., Miller, G. S., & Saylor, J. H.

(2003). Modeling wind-driven circulation during the March 1998 sediment resuspension event in Lake Michigan. *Journal of Geophysical Research: Oceans*, *108*(C2), n/a-n/a. https://doi.org/10.1029/2001JC001159

Beletsky, D., Schwab, D., & McCormick, M. (2006a). Modeling the 1998-2003 summer circulation and thermal structure in Lake Michigan. *Journal of Geophysical Research: Oceans*, *111*(10), 1–18. https://doi.org/10.1029/2005JC003222

Beletsky, D., Schwab, D., & McCormick, M. (2006b). Modeling the 1998–2003 summer circulation and thermal structure in Lake Michigan. *Journal of Geophysical Research*, *111*(C10), C10010. https://doi.org/10.1029/2005JC003222

Booij, N., Ris, R. C., & Holthuijsen, L. H. (1999). A third-generation wave model for coastal regions: 1. Model description and validation. *Journal of Geophysical Research: Oceans*, *104*(C4), 7649–7666. https://doi.org/10.1029/98JC02622

Booij, N., Haagsma, I. J. G., Holthuijsen, L. H., Kieftenburg, A. T. M. M., Ris, R. C., van der Westhuysen, A. J., & Zijlema, M. (2004). *SWAN Cycle III version 40.51 Technical documentation*. Delft, The Netherlands.

Bravo, H.R., Hamidi, S. A., Klump, J. V., & Waples, J. T. (2017). Physical Drivers of the Circulation and Thermal Regime Impacting Seasonal Hypoxia in Green Bay, Lake Michigan. In *Modeling Coastal Hypoxia* (pp. 23–47). Cham: Springer International Publishing. https://doi.org/10.1007/978-3-319-54571-4_2

Bravo, Hector R., Hamidi, S. A., Anderson, E. J., Klump, J. V., & Khazaei, B. (2019). Timescales of Transport Through Lower Green Bay. *Journal of Great Lakes Research*, (In Press.). https://doi.org/https://doi.org/10.1016/j.jglr.2020.06.010

Bravo, Hector R, Hamidi, S. A., Klump, J. V., & Waples, J. T. (2015). Currents and heat fluxes induce stratification leading to hypoxia in Green Bay, Lake Michigan. *E-Proceedings of the 36th IAHR World Congress*, (1985), 1–10.

Chen, C., Liu, H., & Beardsley, R. C. (2003). An unstructured grid, finite-volume, three-dimensional, primitive equations ocean model: Application to coastal ocean and estuaries. *Journal of Atmospheric and Oceanic Technology*, *20*(1), 159–186. https://doi.org/10.1175/1520-0426(2003)020<0159:AUGFVT>2.0.CO;2

1097 Chen, C., Wang, L., Ji, R., Budd, J. W., Schwab, D. J., Beletsky, D., et al. (2004). Impacts of
1098 suspended sediment on the ecosystem in Lake Michigan: A comparison between the 1998
1099 and 1999 plume events. *Journal of Geophysical Research*, *109*(C10), C10S05.
1100 https://doi.org/10.1029/2002JC001687

1101 Chen, C., Huang, H., Beardsley, R. C., Liu, H., Xu, Q., & Cowles, G. (2007). A finite volume
1102 numerical approach for coastal ocean circulation studies: Comparisons with finite difference
1103 models. *Journal of Geophysical Research*, *112*(C3), C03018.
1104 https://doi.org/10.1029/2006JC003485

1105 Chen, C., Beardsley, R. C., Cowles, G., Qi, J., Lai, Z., Gao, G., et al. (2013). *An Unstructured*
1106 *Grid , Finite-Volume Community Ocean Model FVCOM User Manual*. Retrieved from
1107 http://fvcom.smast.umassd.edu/

1108 Chen, T., Zhang, Q., Wu, Y., Ji, C., Yang, J., & Liu, G. (2018). Development of a wave-current
1109 model through coupling of FVCOM and SWAN. *Ocean Engineering*, *164*, 443–454.
1110 https://doi.org/10.1016/J.OCEANENG.2018.06.062

1111 Deines, K. L. (1999). Backscatter estimation using broadband acoustic Doppler current profilers.
1112 *Proceedings of the IEEE Working Conference on Current Measurement*, 249–253.
1113 https://doi.org/10.1109/ccm.1999.755249

1114 Eadie, B. J., Bell, G. L., & Hawley, N. (1991). *Sediment Trap Study in the Green Bay Mass*
1115 *Balance Program: Mass and Organic Carbon Fluxes, Resuspension, and Particle Settling*
1116 *Velocities*. NOAA Technical Memorandum ERL GLERL-75. Great Lakes Environmental
1117 Research Laboratory Ann Arbor, Michigan July 1991.

1118 Fillingham, J. (2015). *Modeling Lake Michigan Nearshore Carbon and Phosphorus Dynamics*.
1119 *Theses and Dissertations*. University of Wisconsin-Milwaukee. Retrieved from
1120 http://dc.uwm.edu/etd/871

1121 García, M. H. (2008). Sediment Transport and Morphodynamics. In M. H. García (Ed.),
1122 *Sedimentation Engineering: Processes, Measurements, Modeling, and Practice* (pp. 21–
1123 163). Reston, VA: American Society of Civil Engineers.
1124 https://doi.org/10.1061/9780784408148.ch02

1125 Ge, J., Torres, R., Chen, C., Liu, J., Xu, Y., Bellerby, R., et al. (2020). Influence of suspended

sediment front on nutrients and phytoplankton dynamics off the Changjiang Estuary: A FVCOM-ERSEM coupled model experiment. *Journal of Marine Systems*, *204*, 103292. https://doi.org/10.1016/j.jmarsys.2019.103292

GLOS. (2021). Data | Great Lakes Observing System. Retrieved January 25, 2021, from https://uwm.edu/glos/data/

Grunert, B. K., Brunner, S. L., Hamidi, S. A., Bravo, H. R., & Klump, J. V. (2018). Quantifying the influence of cold water intrusions in a shallow, coastal system across contrasting years: Green Bay, Lake Michigan. *Journal of Great Lakes Research*, *44*(5), 851–863. https://doi.org/10.1016/J.JGLR.2018.07.009

Guerra, M., Cienfuegos, R., Thomson, J., & Suarez, L. (2017). Tidal energy resource characterization in Chacao Channel, Chile. *International Journal of Marine Energy*, *20*, 1–16. https://doi.org/10.1016/J.IJOME.2017.11.002

Hamidi, Sajad Ahamd, Bravo, H. R., & Klump, J. V. (2013). Evidence of Multiple Physical Drivers on the Circulation and Thermal Regime in the Green Bay of Lake Michigan. In *World Environmental and Water Resources Congress 2013* (pp. 1719–1726). Reston, VA: American Society of Civil Engineers. https://doi.org/10.1061/9780784412947.169

Hamidi, Sajad Ahmad, Bravo, H. R., Val Klump, J., & Waples, J. T. (2015). The role of circulation and heat fluxes in the formation of stratification leading to hypoxia in Green Bay, Lake Michigan. *Journal of Great Lakes Research*, *41*(4), 1024–1036. https://doi.org/10.1016/j.jglr.2015.08.007

Hamidi, Sajad Ahmad, Hosseiny, H., Ekhtari, N., & Khazaei, B. (2017). Using MODIS remote sensing data for mapping the spatio-temporal variability of water quality and river turbid plume. *Journal of Coastal Conservation*, *21*(6), 939–950. https://doi.org/10.1007/s11852-017-0564-y

Harris, C. K., & Wiberg, P. L. (2001). A two-dimensional, time-dependent model of suspended sediment transport and bed reworking for continental shelves. *Computers & Geosciences*, *27*(6), 675–690. https://doi.org/10.1016/S0098-3004(00)00122-9

Harris, V. A., & Christie, J. (1987). *The lower Green Bay Remedial Action Plan: nutrient and eutrophication management. Technical Advisory Committee report*. Publication No. WR-

167-87. Wisconsin Department of Natural Resources. Madison, WI.

Hasselmann, K., Barnett, T. P., Bouws, E., Carlson, H. K., Cartwright, D. E., Enke, K., et al. (1973). Measurements of wind-wave growth and swell decay during the Joint North Sea Wave Project (JONSWAP).

Hasselmann, S., Hasselmann, K., Allender, J. H., & Barnett, T. P. (1985). Computations and Parameterizations of the Nonlinear Energy Transfer in a Gravity-Wave Specturm. Part II: Parameterizations of the Nonlinear Energy Transfer for Application in Wave Models. *Journal of Physical Oceanography*, *15*(11), 1378–1391. https://doi.org/10.1175/1520-0485(1985)015<1378:CAPOTN>2.0.CO;2

Hawley, N., & Niester, J. (1993). Measurement of Horizontal Sediment Transport in Green Bay, May-October, 1989. *Journal of Great Lakes Research*, *19*(2), 368–378. https://doi.org/10.1016/S0380-1330(93)71225-3

Hawley, N., Lesht, B. M., & Schwab, D. J. (2004). A comparison of observed and modeled surface waves in southern Lake Michigan and the implications for models of sediment resuspension. *Journal of Geophysical Research*, *109*(C10), C10S03. https://doi.org/10.1029/2002JC001592

Le Hir, P., Cayocca, F., & Waeles, B. (2011). Dynamics of sand and mud mixtures: A multiprocess-based modelling strategy. *Continental Shelf Research*, *31*(10 SUPPL.), S135–S149. https://doi.org/10.1016/j.csr.2010.12.009

Huang, H., Chen, C., Cowles, G. W., Winant, C. D., Beardsley, R. C., Hedstrom, K. S., & Haidvogel, D. B. (2008). FVCOM validation experiments: Comparisons with ROMS for three idealized barotropic test problems. *Journal of Geophysical Research*, *113*(C7), C07042. https://doi.org/10.1029/2007JC004557

HydroQual Inc. (1999). *Hydrodynamics, Sediment Transport, and Sorbent Dynamics in Green Bay*. Report to Wisconsin Department of Natural Resources, Madison, Wisconsin.

Ji, R., Chen, C., Budd, J. W., Schwab, D. J., Beletsky, D., Fahnenstiel, G. L., et al. (2002). Influences of suspended sediments on the ecosystem in Lake Michigan: A 3-D coupled bio-physical modeling experiment. *Ecological Modelling*, *152*(2–3), 169–190. https://doi.org/10.1016/S0304-3800(02)00027-3

1184 Jones, C. A. (2000). *An Accurate Model of Sediment Transport*. University of California, Santa
1185 Barbara.

1186 Kaster, J. L., Groff, C. M., Klump, J. V., Rupp, D. L., Iyer, S., Hansen, A., et al. (2018).
1187 Evaluation of lower Green Bay benthic fauna with emphasis on re-ecesis of Hexagenia
1188 mayfly nymphs. *Journal of Great Lakes Research*, *44*(5), 895–909.
1189 https://doi.org/10.1016/J.JGLR.2018.06.006

1190 Khazaei, B. (2020). *Development of a Hydrodynamic and Sediment Transport Model for Green*
1191 *Bay, Lake Michigan*. University of Wisconsin-Milwaukee.

1192 Khazaei, B., & Wu, C. (2018). Estimation of Vegetation Coverage Based on Seasonal
1193 Variabilities in MODIS-Based Vegetation Indices. In *World Environmental and Water*
1194 *Resources Congress 2018* (pp. 11–20). Reston, VA: American Society of Civil Engineers.
1195 https://doi.org/10.1061/9780784481400.002

1196 Khazaei, B., Hamidi, S. A., & Nabizadeh, A. (2018). An Empirical Approach to Estimate Total
1197 Suspended Sediment using Observational Data in Fox River and Southern Green Bay, WI.
1198 In *World Environmental and Water Resources Congress*. Minneapolis, MN, USA.

1199 Klump, J. Val, Fitzgerald, S. A., & Waplesa, J. T. (2009). Benthic biogeochemical cycling,
1200 nutrient stoichiometry, and carbon and nitrogen mass balances in a eutrophic freshwater
1201 bay. *Limnology and Oceanography*, *54*(3), 692–712.
1202 https://doi.org/10.4319/lo.2009.54.3.0692

1203 Klump, J. Val, Bratton, J., Fermanich, K., Forsythe, P., Harris, H. J., Howe, R. W., & Kaster, J.
1204 L. (2018). Green Bay, Lake Michigan: A proving ground for Great Lakes restoration.
1205 *Journal of Great Lakes Research*, *44*(5), 825–828.
1206 https://doi.org/10.1016/J.JGLR.2018.08.002

1207 Klump, J.V. V, Edgington, D. N. N., Sager, P. E. E., & Robertson, D. M. M. (1997).
1208 Sedimentary phosphorus cycling and a phosphorus mass balance for the Green Bay (Lake
1209 Michigan) ecosystem. *Canadian Journal of Fisheries and Aquatic Sciences*, *54*(1), 10–26.
1210 Retrieved from http://www.nrcresearchpress.com/doi/10.1139/f96-247

1211 Klump, J .Val, Brunner, S. L., Grunert, B. K., Kaster, J. L., Weckerly, K., Houghton, E. M., et al.
1212 (2018). Evidence of persistent, recurring summertime hypoxia in Green Bay, Lake

1213 Michigan. *Journal of Great Lakes Research*, *44*(5), 841–850.
1214 https://doi.org/10.1016/J.JGLR.2018.07.012

1215 Komen, G. J., Hasselmann, K., & Hasselmann, K. (1984). On the Existence of a Fully
1216 Developed Wind-Sea Spectrum. *Journal of Physical Oceanography*, *14*(8), 1271–1285.
1217 https://doi.org/10.1175/1520-0485(1984)014<1271:OTEOAF>2.0.CO;2

1218 Labuhn, S. L. (2017). *Dissolved oxygen dynamics within Green Bay in an effort to understand*
1219 *hypoxia Table of Contents*. University of Wisconsin-Milwaukee.

1220 Lai, W., Pan, J., & Devlin, A. T. (2018). Impact of tides and winds on estuarine circulation in the
1221 Pearl River Estuary. *Continental Shelf Research*, *168*, 68–82.
1222 https://doi.org/10.1016/J.CSR.2018.09.004

1223 Lee, C., Schwab, D. J., & Hawley, N. (2005). Sensitivity analysis of sediment resuspension
1224 parameters in coastal area of southern Lake Michigan. *Journal of Geophysical Research C:*
1225 *Oceans*, *110*(3), 1–16. https://doi.org/10.1029/2004JC002326

1226 Lee, C., Schwab, D. J., Beletsky, D., Stroud, J., & Lesht, B. (2007). Numerical modeling of
1227 mixed sediment resuspension, transport, and deposition during the March 1998 episodic
1228 events in southern Lake Michigan. *Journal of Geophysical Research: Oceans*, *112*(2), 1–17.
1229 https://doi.org/10.1029/2005JC003419

1230 Li, B., Tanaka, K. R., Chen, Y., Brady, D. C., & Thomas, A. C. (2017). Assessing the quality of
1231 bottom water temperatures from the Finite-Volume Community Ocean Model (FVCOM) in
1232 the Northwest Atlantic Shelf region. *Journal of Marine Systems*, *173*, 21–30.
1233 https://doi.org/10.1016/J.JMARSYS.2017.04.001

1234 Li, J., Pan, S., Chen, Y., Fan, Y.-M., & Pan, Y. (2018). Numerical estimation of extreme waves
1235 and surges over the northwest Pacific Ocean. *Ocean Engineering*, *153*, 225–241.
1236 https://doi.org/10.1016/J.OCEANENG.2018.01.076

1237 Lou, J., Schwab, D. J., Beletsky, D., & Hawley, N. (2000). A model of sediment resuspension
1238 and transport dynamics in southern Lake Michigan. *Journal of Geophysical Research:*
1239 *Oceans*, *105*(C3), 6591–6610. https://doi.org/10.1029/1999JC900325

1240 Luo, L., Wang, J., Schwab, D. J., Vanderploeg, H., Leshkevich, G., Bai, X., et al. (2012).
1241 Simulating the 1998 spring bloom in Lake Michigan using a coupled physical-biological

model. *J. Geophys. Res*, *117*, 10011. https://doi.org/10.1029/2012JC008216

Manchester-Neesvig, J. B., Andren, A. W., & Edgington, D. N. (1996). Patterns of Mass Sedimentation and of Deposition of Sediment Contaminated by PCBs in Green Bay. *Journal of Great Lakes Research*, *22*(2), 444–462. https://doi.org/10.1016/S0380-1330(96)70969-3

Mantz, P. A. (1977). Incipient transport of fine grains and flakes by fluids-extended Shields diagram. *Journal of the Hydraulics Division*, *103*(HY6).

Mao, M., & Xia, M. (2017). Dynamics of wave–current–surge interactions in Lake Michigan: A model comparison. *Ocean Modelling*, *110*, 1–20. https://doi.org/10.1016/J.OCEMOD.2016.12.007

Mao, M., & Xia, M. (2020). Monthly and episodic dynamics of summer circulation in Lake Michigan. *Journal of Geophysical Research: Oceans*, *125*(6). https://doi.org/10.1029/2019jc015932

Mao, M., van der Westhuysen, A. J., Xia, M., Schwab, D. J., & Chawla, A. (2016). Modeling wind waves from deep to shallow waters in Lake Michigan using unstructured SWAN. *Journal of Geophysical Research: Oceans*, *121*(6), 3836–3865. https://doi.org/10.1002/2015JC011340

Mellor, G. L., & Yamada, T. (1982). Development of a turbulence closure model for geophysical fluid problems. *Reviews of Geophysics*, *20*(4), 851. https://doi.org/10.1029/RG020i004p00851

Mengual, B., Hir, P., Cayocca, F., & Garlan, T. (2017). Modelling Fine Sediment Dynamics: Towards a Common Erosion Law for Fine Sand, Mud and Mixtures. *Water*, *9*(8), 564. https://doi.org/10.3390/w9080564

Meyer-Peter, E., & Müller, R. (1948). Formulas for Bed-Load transport. *IAHSR 2nd Meeting, Stockholm, Appendix 2*. Retrieved from https://repository.tudelft.nl/islandora/object/uuid%3A4fda9b61-be28-4703-ab06-43cdc2a21bd7

Miller, T. R. (2020). Lakestat. Retrieved November 12, 2019, from http://www.lakestat.com/

1270 Mitchener, H., & Torfs, H. (1996). Erosion of mud/sand mixtures. *Coastal Engineering*, *29*(1–2),
1271 1–25. https://doi.org/10.1016/S0378-3839(96)00002-6

1272 Moore, J. R., Meyer, R. P., & Morgan, C. L. (1973). *Investigation of the Sediments and Potential*
1273 *Manganese Nodule Resources of Green Bay, Wisconsin*. University of Wisconsin, Sea
1274 Grant College Program. Technical Report-WIS. WISCU-T-73-001.

1275 National Geophysical Data Center. (2015). Bathymetric Data Viewer. Retrieved January 1, 2017,
1276 from http://maps.ngdc.noaa.gov/viewers/bathymetry/

1277 NEW Water. (2017). Aquatic Monitoring Program › NEW Water. Retrieved October 1, 2018,
1278 from http://newwater.us/programs-initiatives/aquatic-monitoring-program/

1279 NOAA. (2017). Bathymetry of Lake Michigan. Retrieved January 1, 2017, from
1280 https://ngdc.noaa.gov/mgg/greatlakes/michigan.html

1281 NOAA. (2018). National Centers for Environmental Information (NCEI). Retrieved November
1282 1, 2018, from https://gis.ncdc.noaa.gov/maps/ncei/cdo/hourly

1283 NOAA. (2020). Station Selection - NOAA Tides & Currents. Retrieved January 5, 2020, from
1284 https://tidesandcurrents.noaa.gov/stations.html?type=Water+Levels

1285 Ouillon, S. (2018). Why and How Do We Study Sediment Transport? Focus on Coastal Zones
1286 and Ongoing Methods. *Water*, *10*(4), 390. https://doi.org/10.3390/w10040390

1287 Parker, G. (2004). *1D Morphodynamics of Rivers and Turbidity Currents*. Saint Anthony Falls
1288 Lab., Univ. of Minn., Minneapolis. [Available at
1289 http://hydrolab.illinois.edu/people/parkerg/morphodynamics_e-book.htm].

1290 Qi, J., Chen, C., Beardsley, R. C., Perrie, W., Cowles, G. W., & Lai, Z. (2009). An unstructured-
1291 grid finite-volume surface wave model (FVCOM-SWAVE): Implementation, validations
1292 and applications. *Ocean Modelling*, *28*(1–3), 153–166.
1293 https://doi.org/10.1016/J.OCEMOD.2009.01.007

1294 Qualls, T., Harris, H. J., & Harris, V. (2013). *The State of Green Bay: The Condition of the Bay*
1295 *of Green Bay/Lake Michigan 2013*. University of Wisconsin Sea Grant Institute. Retrieved
1296 from https://www.seagrant.wisc.edu/wp-content/uploads/2018/11/State-of-the-Bay-Report-
1297 2013.pdf

1298 Read, J., Klump, V., Johengen, T., Schwab, D., Paige, K., Eddy, S., et al. (2010). Working in
1299 Freshwater: The Great Lakes Observing System Contributions to Regional and National
1300 Observations, Data Infrastructure, and Decision Support. *Marine Technology Society*
1301 *Journal*, *44*(6), 84–98. https://doi.org/10.4031/MTSJ.44.6.12

1302 Ris, R. C., Holthuijsen, L. H., & Booij, N. (1999). A third-generation wave model for coastal
1303 regions: 2. Verification. *Journal of Geophysical Research: Oceans*, *104*(C4), 7667–7681.
1304 https://doi.org/10.1029/1998JC900123

1305 Rowe, M.D., Anderson, E. J., Wang, J., & Vanderploeg, H. A. (2015). Modeling the effect of
1306 invasive quagga mussels on the spring phytoplankton bloom in Lake Michigan. *Journal of*
1307 *Great Lakes Research*, *41*, 49–65. https://doi.org/10.1016/J.JGLR.2014.12.018

1308 Rowe, Mark D., Anderson, E. J., Vanderploeg, H. A., Pothoven, S. A., Elgin, A. K., Wang, J., &
1309 Yousef, F. (2017). Influence of invasive quagga mussels, phosphorus loads, and climate on
1310 spatial and temporal patterns of productivity in Lake Michigan: A biophysical modeling
1311 study. *Limnology and Oceanography*, *62*(6), 2629–2649. https://doi.org/10.1002/lno.10595

1312 Safaie, A., Wendzel, A., Ge, Z., Nevers, M. B., Whitman, R. L., Corsi, S. R., & Phanikumar, M.
1313 S. (2016). Comparative Evaluation of Statistical and Mechanistic Models of *Escherichia*
1314 *coli* at Beaches in Southern Lake Michigan. *Environmental Science & Technology*, *50*(5),
1315 2442–2449. https://doi.org/10.1021/acs.est.5b05378

1316 Sanford, L. P. (2008). Modeling a dynamically varying mixed sediment bed with erosion,
1317 deposition, bioturbation, consolidation, and armoring. *Computers and Geosciences*, *34*(10),
1318 1263–1283. https://doi.org/10.1016/j.cageo.2008.02.011

1319 Schwab, D.J., & Beletsky, D. (1998). *Lake Michigan Mass Balance Study: Hydrodynamic*
1320 *Modeling Project. ERL GLERL-108*. NOAA GLERL, Ann Arbor, MI.

1321 Schwab, David J. (1983). Numerical Simulation of Low-Frequency Current Fluctuations in Lake
1322 Michigan. *Journal of Physical Oceanography*, *13*(12), 2213–2224.
1323 https://doi.org/10.1175/1520-0485(1983)013<2213:NSOLFC>2.0.CO;2

1324 Shen, C. (2016). *Modeling of dreissenid mussel impacts on Lake Michigan*. *ProQuest*
1325 *Dissertations and Theses*. University of Wisconsin-Milwaukee. Retrieved from
1326 https://search.proquest.com/docview/1844987331?accountid=6180%0Ahttp://dw2zn6fm9z.

search.serialssolution.com?ctx_ver=Z39.88-2004&ctx_enc=info:ofi/enc:UTF-8&rfr_id=info:sid/ProQuest+Dissertations+%26+Theses+Global&rft_val_fmt=info:ofi/fmt:kev:mtx:dissertat

Sherwood, C. R., Aretxabaleta, A. L., Harris, C. K., Paul Rinehimer, J., Verney, R., & Ferré, B. (2018). Cohesive and mixed sediment in the Regional Ocean Modeling System (ROMS v3.6) implemented in the Coupled Ocean-Atmosphere-Wave-Sediment Transport Modeling System (COAWST r1234). *Geoscientific Model Development*, *11*(5), 1849–1871. https://doi.org/10.5194/gmd-11-1849-2018

Shore, J. A. (2009). Modelling the circulation and exchange of Kingston Basin and Lake Ontario with FVCOM. *Ocean Modelling*, *30*(2–3), 106–114. https://doi.org/10.1016/J.OCEMOD.2009.06.007

Smagorinsky, J. (1963). General circulation experiments with the primitive equations, I. The basic experiment. *Monthly Weather Review*, *91*(3), 99–164. https://doi.org/10.1175/1520-0493(1963)091<0099:GCEWTP>2.3.CO;2

Soulsby, R. L. (1998). Dynamics of marine sands.

Velleux, M., Endicott, D., Steuer, J., Jaeger, S., & Patterson, D. (1995). Long-Term Simulation of PCB Export from the Fox River to Green Bay. *Journal of Great Lakes Research*, *21*(3), 359–372. https://doi.org/10.1016/S0380-1330(95)71047-4

Waples, J. T., & Klump, J. V. (2002). Biophysical effects of a decadal shift in summer wind direction over the Laurentian Great Lakes. *Geophysical Research Letters*, *29*(8), 43-1-43–4. https://doi.org/10.1029/2001GL014564

Warner, J. C., Sherwood, C. R., Signell, R. P., Harris, C. K., & Arango, H. G. (2008). Development of a three-dimensional, regional, coupled wave, current, and sediment-transport model. *Computers & Geosciences*, *34*(10), 1284–1306. https://doi.org/10.1016/J.CAGEO.2008.02.012

Wisconsin DNR. (2000). *Model Evaluation Workgroup Technical Memorandum 2f: Estimation of Sediment Bed Properties for Green Bay*.

Wolanski, E. (2007). Estuarine sediment dynamics. In *Estuarine Ecohydrology* (pp. 41–69). Elsevier. https://doi.org/10.1016/b978-044453066-0.50004-0

1356 Wolanski, E., & Elliott, M. (2015). *Estuarine Ecohydrology: An Introduction*. *Estuarine*
1357 *Ecohydrology*. Elsevier. https://doi.org/10.1016/c2013-0-13014-0

1358 Xue, P., Schwab, D. J., & Hu, S. (2015). An investigation of the thermal response to
1359 meteorological forcing in a hydrodynamic model of Lake Superior. Retrieved from
1360 https://www.semanticscholar.org/paper/An-investigation-of-the-thermal-response-to-
1361 forcing-Xue-Schwab/40eca7b276ebcad8589f9df017dbd724b1ffc00d

1362 Yolcubal, I., Brusseau, M. L., Artiola, J. F., Wierenga, P., & Wilson, L. G. (2004).
1363 ENVIRONMENTAL PHYSICAL PROPERTIES AND PROCESSES. *Environmental*
1364 *Monitoring and Characterization*, 207–239. https://doi.org/10.1016/B978-012064477-
1365 3/50014-X

1366 Zhang, J., Xiong, M., Yin, C., & Gan, S. (2018). Inner shelf response to storm track variations
1367 over the east LeiZhou Peninsula, China. *International Journal of Applied Earth*
1368 *Observation and Geoinformation*, *71*, 56–69. https://doi.org/10.1016/J.JAG.2018.03.011

1369

Figure 1.

Great Lakes Basin

Chambers Island

Menominee River

04067500

Green Bay

A'

C'

B

C

B'

Green Bay Connecting Straits

Green Island

Sturgeon Bay

A

40851385

Fox River

N

W

E

S

0 12½ 25 50 Km

Station Name	Station ID	Lat	Lon
Southern Green Bay Buoy	45014	44.80	-87.76
Milwaukee Atwater 20m Buoy	45013	43.10	-87.85
Northern Michigan Buoy	45002	45.34	-86.41
Southern Michigan Buoy	45007	42.67	-87.03
Sleeping Bear Dunes Buoy	45183	44.98	-85.83
Green Bay West Buoy	GBW	44.58	-87.99
Green Bay East Buoy	GBE	44.55	-87.96
NEW Water Station 13	NW13	44.53	-88.01
USGS Fox River Gauge	40851385	44.53	-88.01
USGS Menominee River Gauge	04067500	45.33	-87.66
USGS Lake Michigan at Gary	04092788	41.65	-87.43
USGS Lake Michigan at Hyde Park	04092440	41.78	-87.57

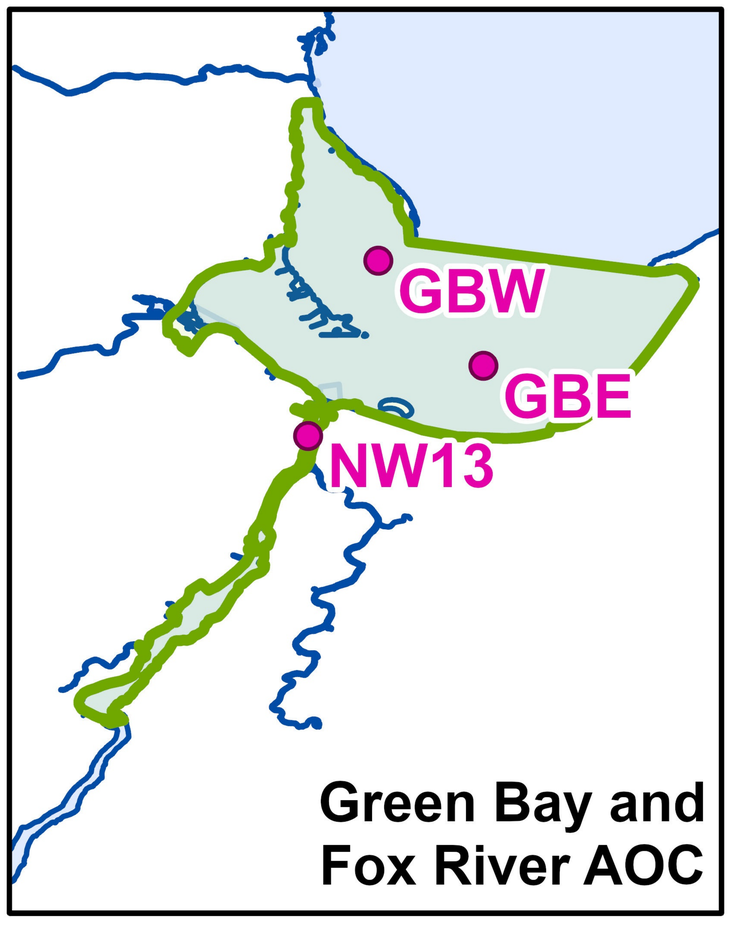

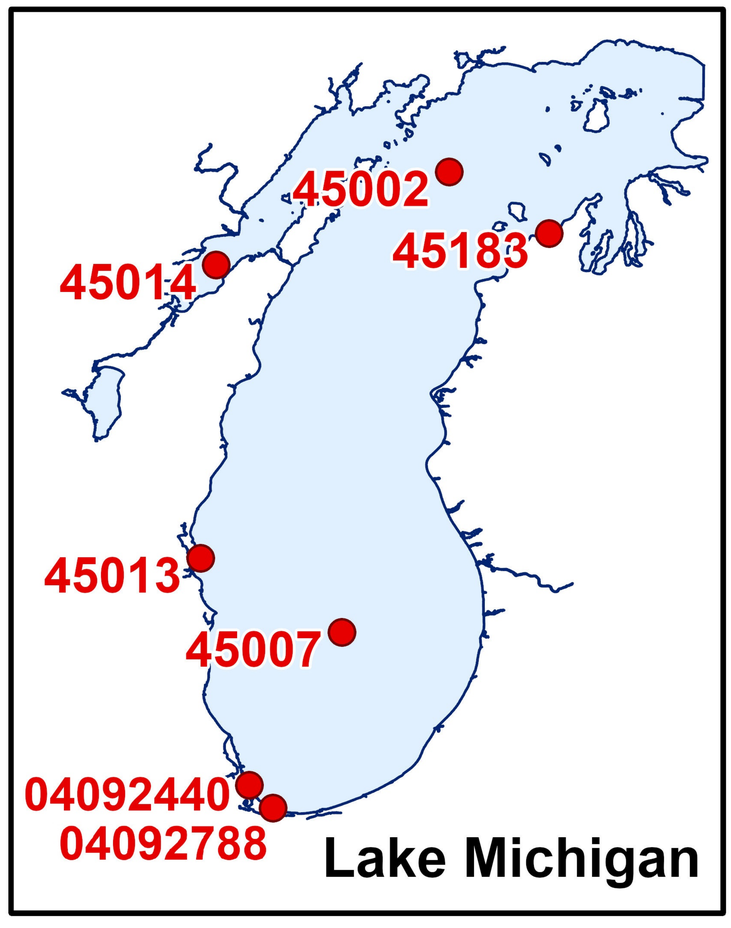

Figure 2.

45014 45013 45007 45002

u_{surf} (m/s)
u_{botm} (m/s)
W_{Hs} (m)
W_{dir} (degrees)
TW_{surf} (°C)
TW_{botm} (°C)
TSS (mg/L)

Predicted Values

Observed Values

GBE GBW 04092788 04092440 45183

Figure 3.

MODIS

May-07 | Jun-05 | Jul-16

Aug-11 | Sep-12 | Oct-16

FVCOM

May-07 | Jun-05 | Jul-16

Aug-11 | Sep-12 | Oct-16

45.2
45.1
45.0
44.9
44.8
44.7
44.6
44.5

-88 -87.8 -87.6 -87.4 -87.2

TSS (mg/L)

20
18
16
14
12
10
8
6
4
2
0

Figure 4.

TSS profile in lower Green Bay (45014 buoy)

Depth (m)

Observed

0
-2
-4
-6
-8
-10
-12

Predicted

0
-2
-4
-6
-8
-10
-12

Jul

Aug

Sep

2018

0 1 2 3 4 5 6 7 8 9 10

TSS (mg/L)

Figure 5.

Lake Michigan

May
June
July
August
September
October

Green Bay

May
June
July
August
September
October

W_{spd}: 5 m/s

Figure 6.

Lake Michigan

Green Bay

May

June

July

August

September

October

46.0
45.5
45.0
44.5
44.0
43.5
43.0
42.5
42.0
41.5

-88
-87.5
-87
-86.5
-86
-85

0.1
0.09
0.08
0.07
0.06
0.05
0.04
0.03
0.02
0.01
0

u_{spd} (m/s)

Figure 7.

A
A'
B
B'
C
C'
May
June
July
August
September
October
0
-20
-40
Depth (m)
0
40
80
120
160
0
10
20
0
20
40
Distance (km)
-0.05
-0.04
-0.03
-0.02
-0.01
0
0.01
0.02
0.03
0.04
0.05
u_{spd} (m/s)

Figure 8.

Lake Michigan

May

June

July

August

September

October

Green Bay

May

June

July

August

September

October

46.0
45.5
45.0
44.5
44.0
43.5
43.0
42.5
42.0
41.5

-88
-87.5
-87
-86.5
-86
-85

1
0.9
0.8
0.7
0.6
0.5
0.4
0.3
0.2
0.1
0

W_{Hs} (m)

Figure 9.

Lake Michigan

Green Bay

May

June

July

August

September

October

46.0
45.5
45.0
44.5
44.0
43.5
43.0
42.5
42.0
41.5

-88
-87.5
-87
-86.5
-86
-85

50
45
40
35
30
25
20
15
10
5
0

τ_{sf} ($\times 10^{-3}$ N/m^2)

Figure 10.

Lake Michigan

May
June
July
August
September
October

Green Bay

May
June
July
August
September
October

46.0
45.5
45.0
44.5
44.0
43.5
43.0
42.5
42.0
41.5

-88
-87.5
-87
-86.5
-86
-85

TW (°C)
30
25
20
15
10
5
0

Figure 11.

A
A'
B
B'
C
C'
May
June
July
August
September
October
Depth (m)
0
-20
-40
0
40
80
120
160
0
10
20
0
20
40
Distance (km)
TW (˚C)
0
5
10
15
20
25
30

Figure 12.

Lake Michigan

Green Bay

May

June

July

August

September

October

46.0
45.5
45.0
44.5
44.0
43.5
43.0
42.5
42.0
41.5

-88
-87
-86
-85

-87.5
-87
-86.5

TSS (mg/L)

20
18
16
14
12
10
8
6
4
2
0

Figure 13.

A
A'
B
B'
C
C'
May
June
July
August
September
October
0
-20
-40
Depth (m)
0
40
80
120
160
0
10
20
0
20
40
Distance (km)
TSS (mg/L)
0
2
4
6
8
10
12
14
16
18
20

Figure 14.

2016 2017 2018 2019 Average

46 45 44 43 42

W_{spd}: 2.5 m/s

50 40 30 20 10 0

τ_{sf} ($\times 10^{-3}$ N/m^2)

30 20 10 0

TW ($^{\circ}$C)

20 15 10 5 0

TSS (mg/L)

-88 -86

Figure S1.

Lake Michigan Bathymetry (m)

280.0
245.0
210.0
175.0
140.0
105.0
70.0
35.0
0.0

Green Bay Bathymetry (m)

50.0
40.0
30.0
20.0
10.0
0.0

Figure S2.

Little Summer Island
Fairport
St. Martin Island
Summer Island
Poverty Island
Washington Island
Plum Island
Rock Island
Detroit Island
Northport
N
W
E
S
0
10
20
Km
Little Suamico River
Little Tail Point
Suamico River
Long Tail Point
Cat Island
Duck Creek
Bay Beach Island
Fox River
East River
N
W
E
S
0
4
8
Km

Figure S3.

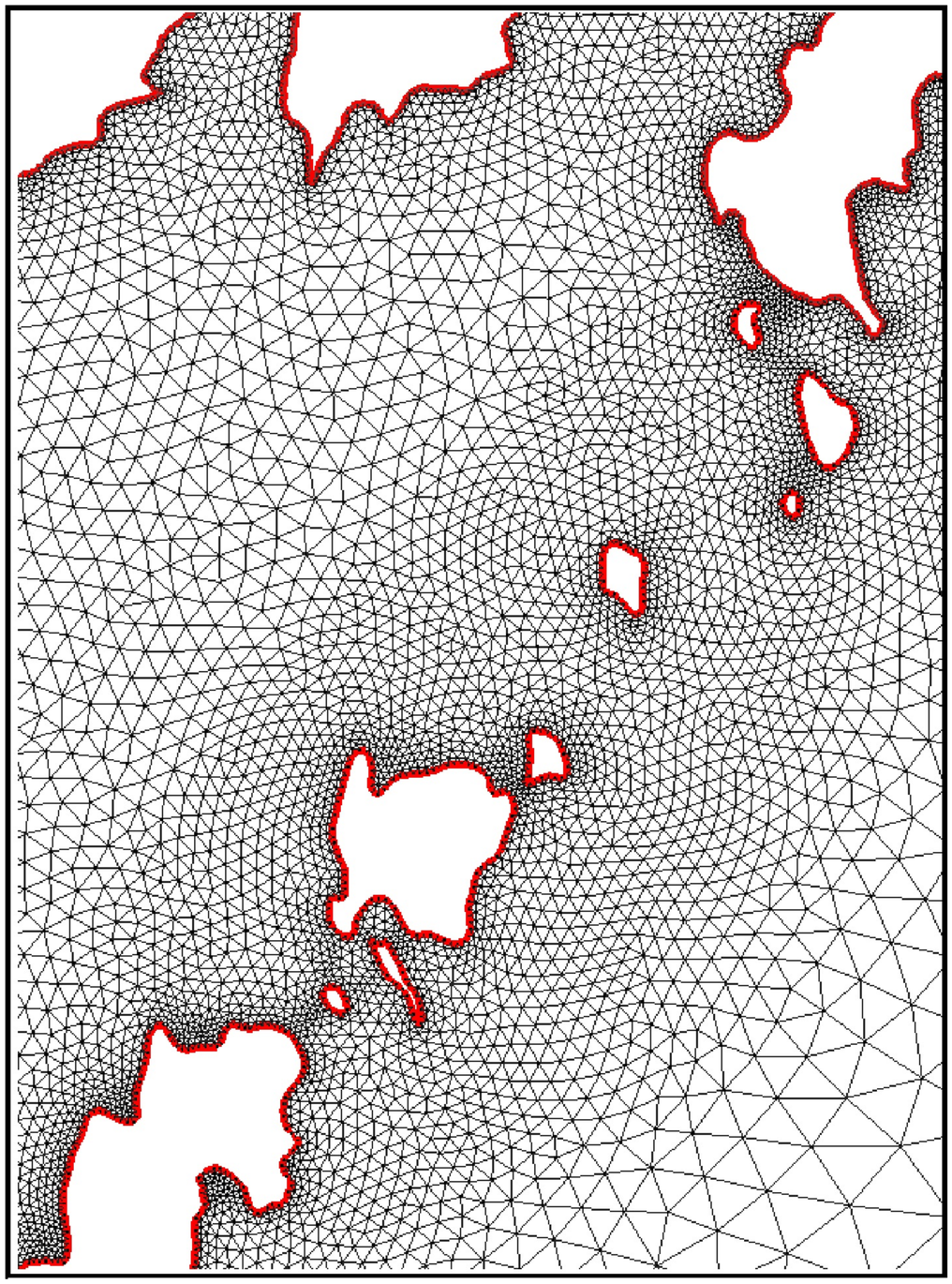

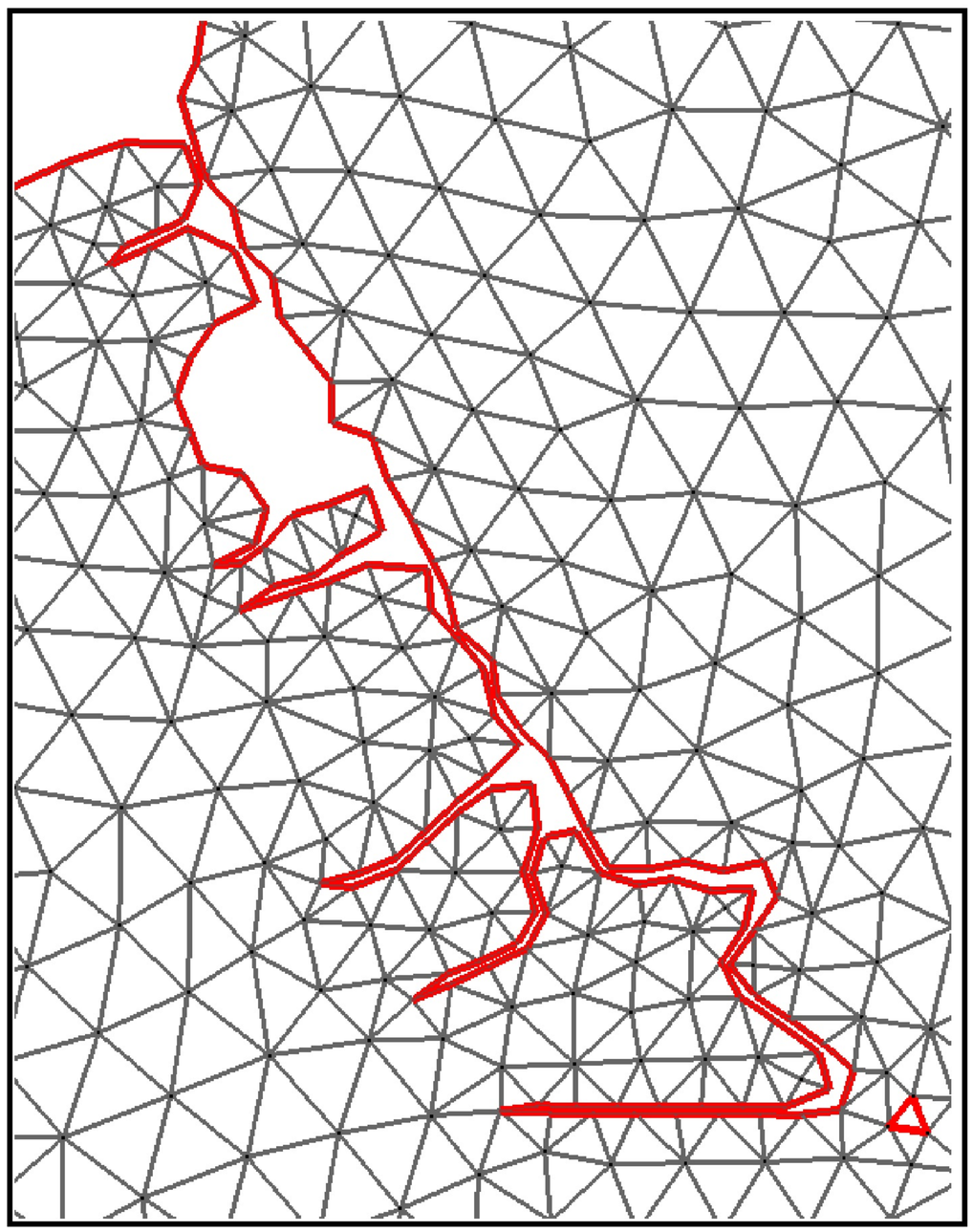

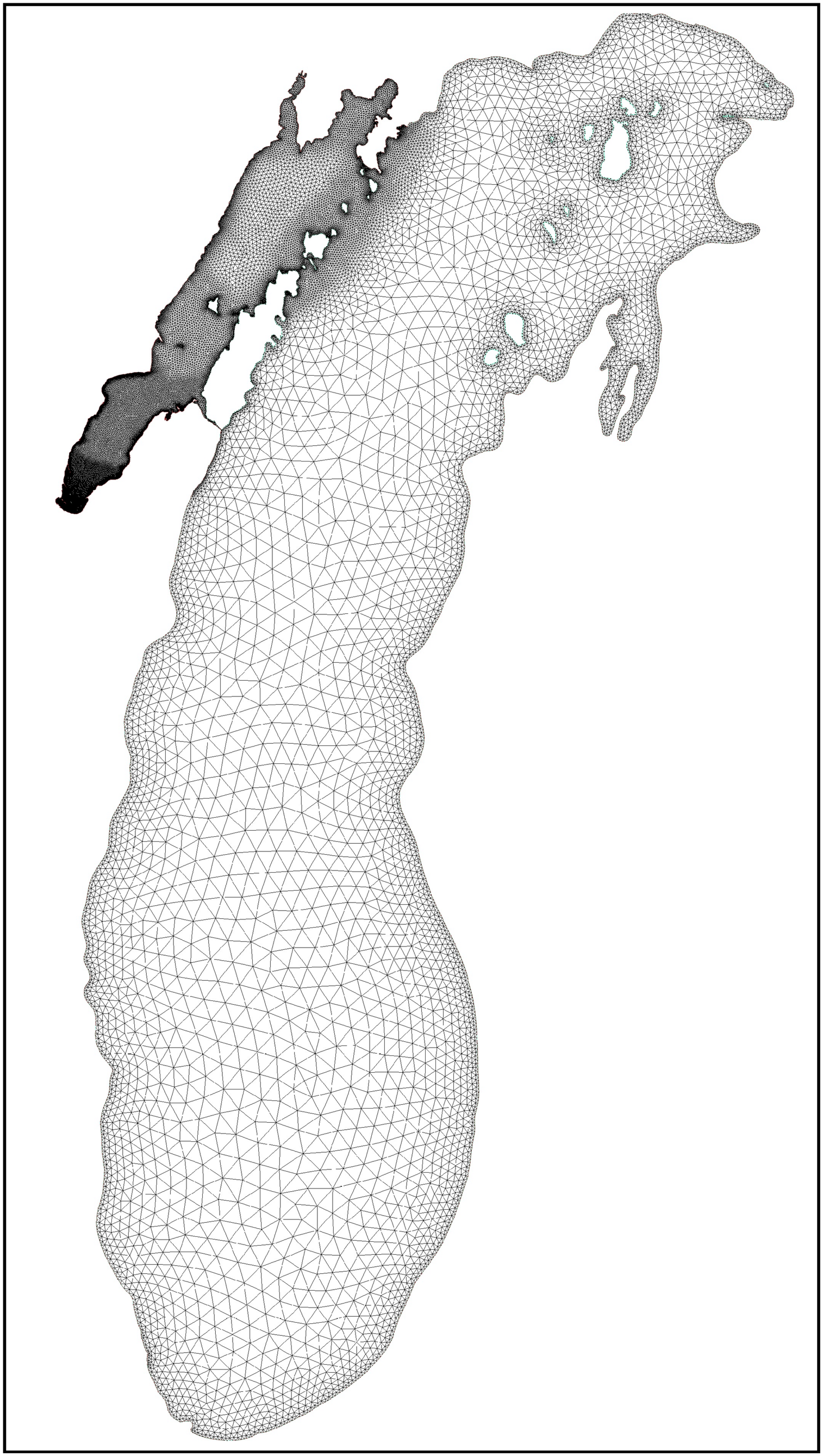

Figure S4.

46
45.5
45
44.5
44
43.5
43
42.5
42
41.5
-88
-87
-86
-85
Cohesive Sediments
Non-cohesive Sediments
Percentage
0
20
40
60
80
100

Figure S5.

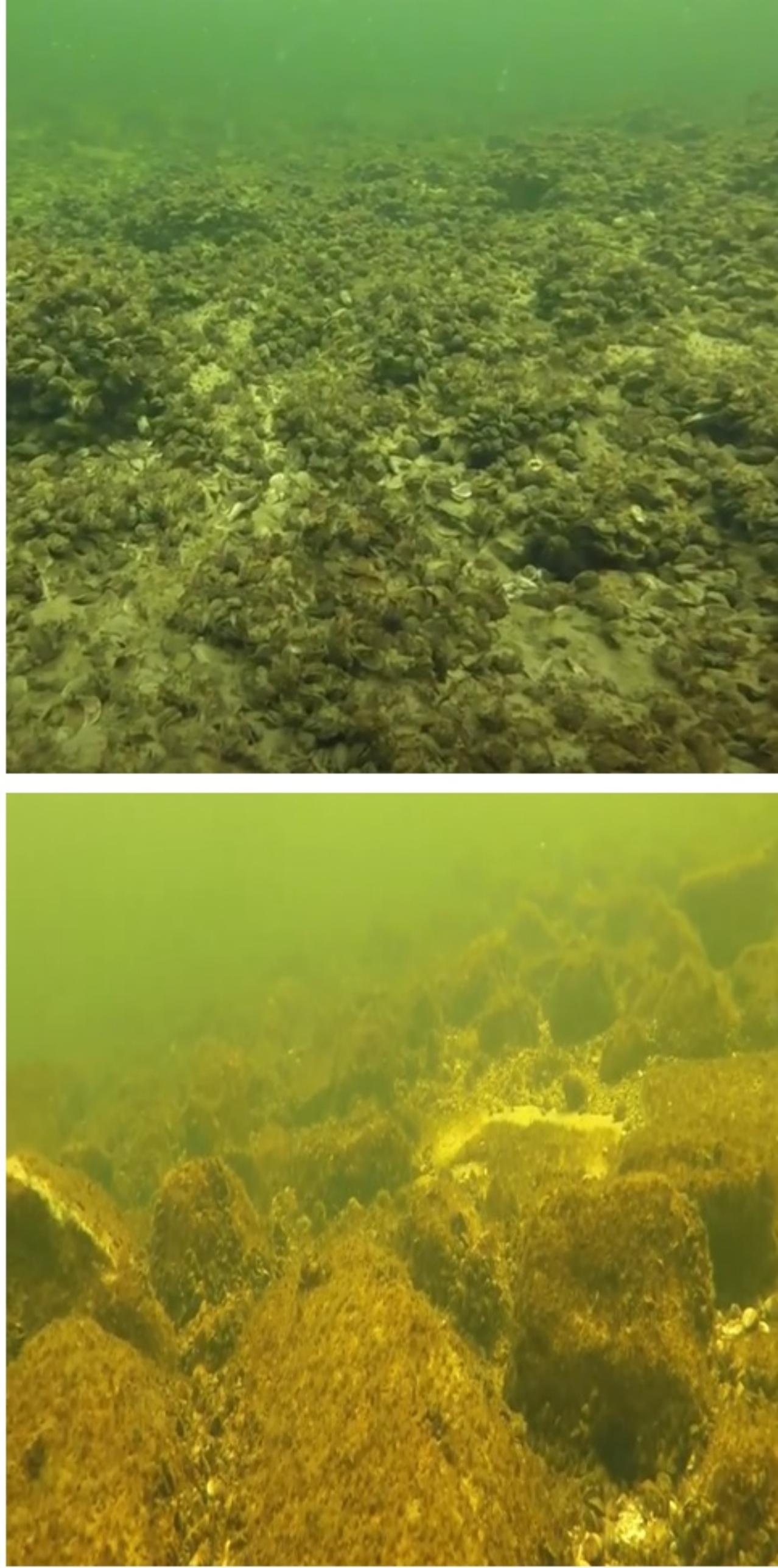

Figure S6.

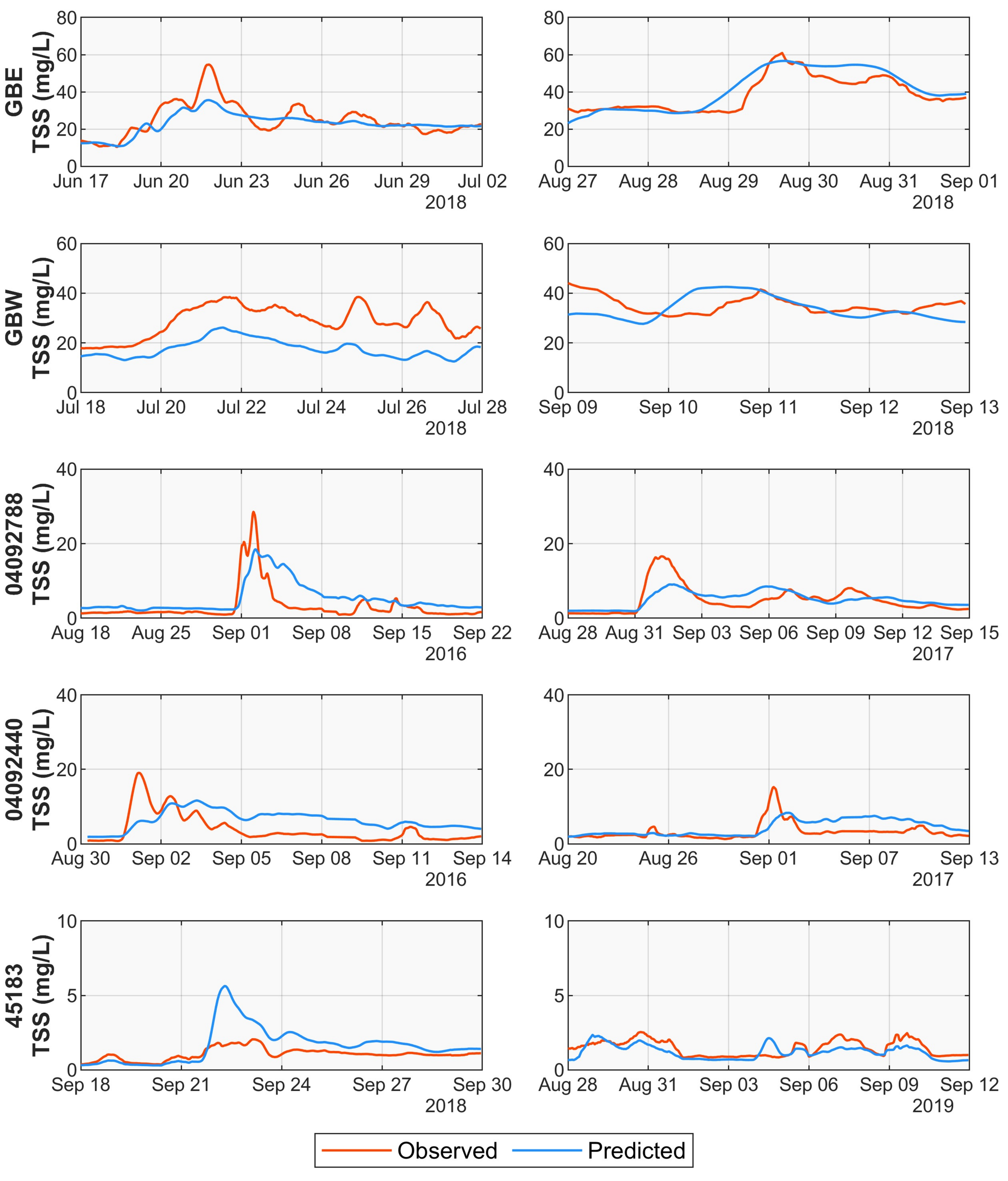
GBE
TSS (mg/L)
80
60
40
20
0
Jun 17
Jun 20
Jun 23
Jun 26
Jun 29
Jul 02
2018
Aug 27
Aug 28
Aug 29
Aug 30
Aug 31
Sep 01
2018
GBW
TSS (mg/L)
60
40
20
0
Jul 18
Jul 20
Jul 22
Jul 24
Jul 26
Jul 28
2018
Sep 09
Sep 10
Sep 11
Sep 12
Sep 13
2018
04092788
TSS (mg/L)
40
20
0
Aug 18
Aug 25
Sep 01
Sep 08
Sep 15
Sep 22
2016
Aug 28
Aug 31
Sep 03
Sep 06
Sep 09
Sep 12
Sep 15
2017
04092440
TSS (mg/L)
40
20
0
Aug 30
Sep 02
Sep 05
Sep 08
Sep 11
Sep 14
2016
Aug 20
Aug 26
Sep 01
Sep 07
Sep 13
2017
45183
TSS (mg/L)
10
5
0
Sep 18
Sep 21
Sep 24
Sep 27
Sep 30
2018
Aug 28
Aug 31
Sep 03
Sep 06
Sep 09
Sep 12
2019
Observed
Predicted

Figure S7.

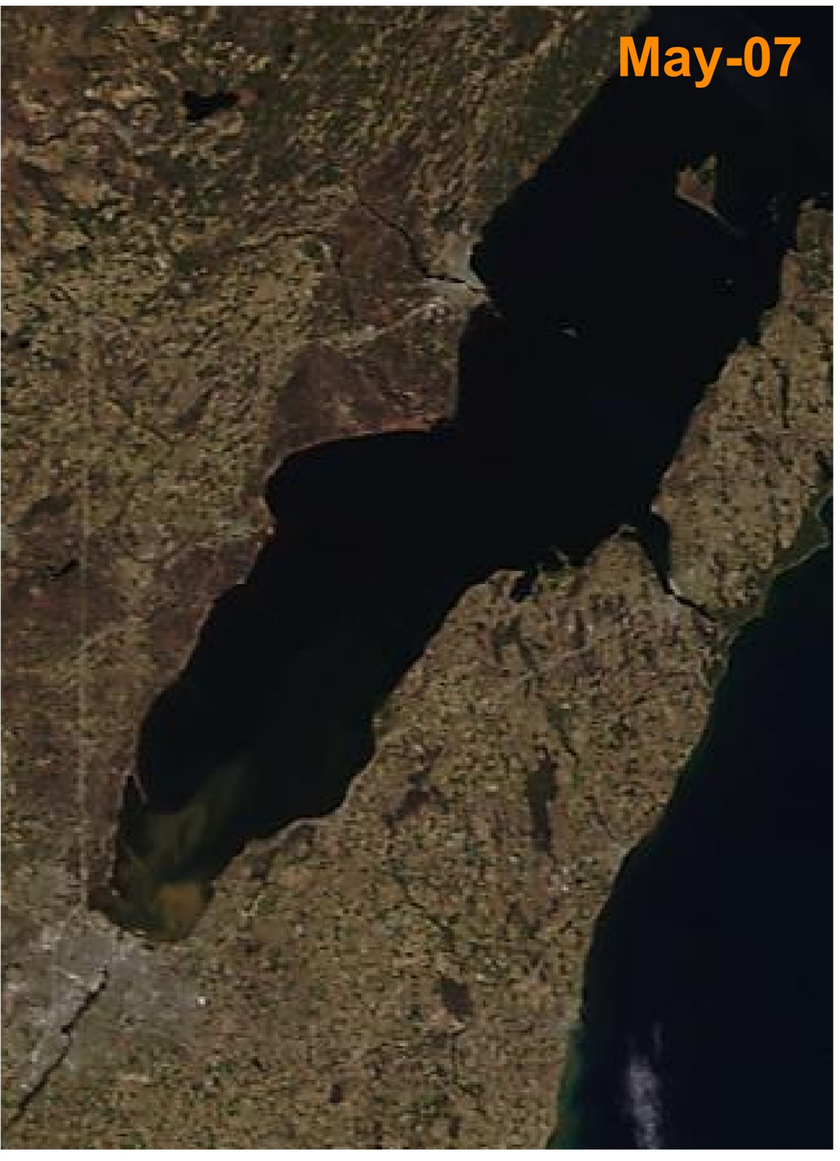
May-07

Jun-05

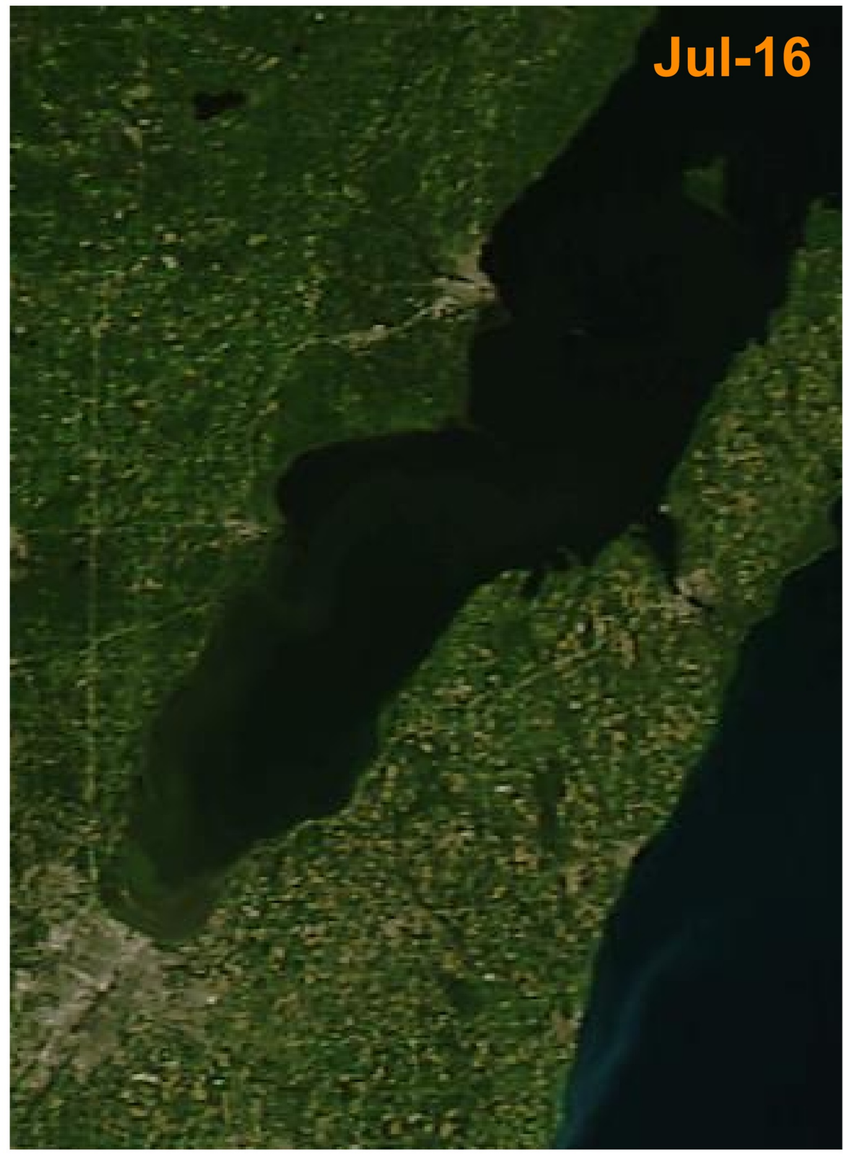
Jul-16

AUG-11

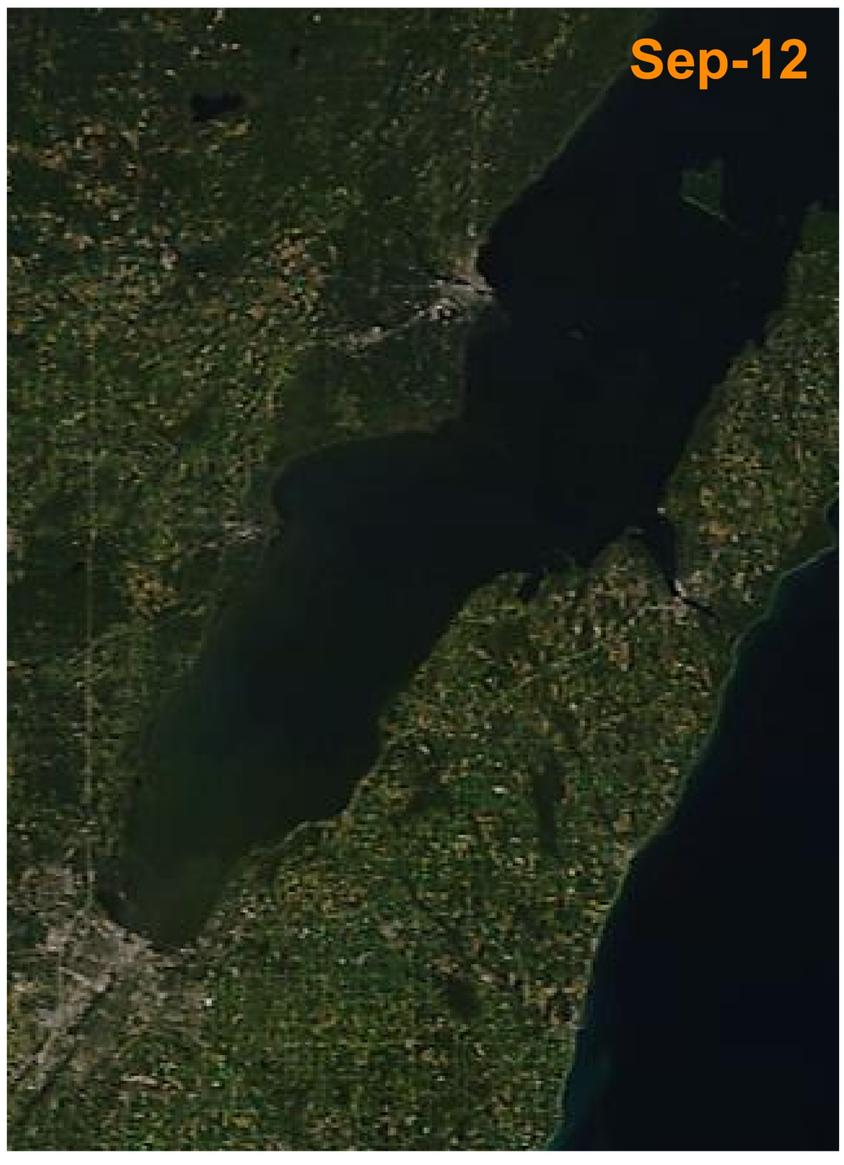
Sep-12

Oct-16

Figure S8.

Lake Michigan

Green Bay

May

June

July

August

September

October

46.0
45.5
45.0
44.5
44.0
43.5
43.0
42.5
42.0
41.5

-88
-87
-86
-85

-87.5
-87
-86.5

0.1
0.09
0.08
0.07
0.06
0.05
0.04
0.03
0.02
0.01
0

u_{spd} (m/s)

Figure S9.

Lake Michigan

Green Bay

May

June

July

August

September

October

46.0
45.5
45.0
44.5
44.0
43.5
43.0
42.5
42.0
41.5

-88
-87.5
-87
-86.5
-86
-85

0.1
0.09
0.08
0.07
0.06
0.05
0.04
0.03
0.02
0.01
0

u_{spd} (m/s)

Figure S10.

Combined currents and waves

Currents only

Lake Michigan

Green Bay

46.0
45.5
45.0
44.5
44.0
43.5
43.0
42.5
42.0
41.5

-88
-87.5
-87
-86.5
-86
-85

50
45
40
35
30
25
20
15
10
5
0

τ_{sf} ($\times 10^{-3}$ N/m^2)

Figure S11.

Combined currents and waves

Currents only

Lake Michigan

Green Bay

46.0
45.5
45.0
44.5
44.0
43.5
43.0
42.5
42.0
41.5

-88
-87.5
-87
-86.5
-86
-85

TSS (mg/L)

20
18
16
14
12
10
8
6
4
2
0

Figure S12.

Date: Jul 13, 2016

Date: Aug 05, 2016

Date: Sep 02, 2016

Wind Fields

5 m/s

Surface Currents

0.25 m/s

Surface Temperature

T (°C)

30

20

10

0

46

45

44

43

42

-88

-87

-86

-85